

Responses of microbial metabolic rates to non-equilibrated silicate vs calcium-based ocean alkalinity enhancement

Laura Marín-Samper¹, Javier Arístegui¹, Nauzet Hernández-Hernández¹, Ulf Riebesell²

¹ Instituto de Oceanografía y Cambio Global, Universidad de Las Palmas de Gran Canaria, 35017 Telde, Spain

² GEOMAR Helmholtz Centre for Ocean Research Kiel, 24148 Kiel, Germany

Correspondence to: Laura Marín-Samper (laura.marin@ulpgc.es), Javier Arístegui (javier.aristegui@ulpgc.es)

Abstract. This study contributes to the inaugural exploration of non-equilibrated ocean alkalinity enhancement (OAE). ~~The manipulation of t~~Total ~~a~~Alkalinity (TA) ~~was manipulated, with,~~ ~~involving~~ silicate and calcium-based Δ TA gradients ranging from 0 to 600 $\mu\text{mol} \cdot \text{L}^{-1}$, ~~was conducted~~ without prior CO_2 sequestration, under natural conditions and at a mesocosm scale ($\sim 60 \text{ m}^3$). ~~The resulting impact. This manipulation led included to an a sustained~~ increase in pH and a decrease in pCO_2 , ~~sustained across throughout~~ the experiment, as full natural equilibration ~~via through~~ sea-air gas exchange did not occur. Implemented in a neritic system under post-bloom conditions, a midway mixing event was simulated. ~~After the inorganic nutrient addition, mild delays in bloom formation were observed. These delays were related, though not directly proportional to, the Δ TA gradient, as indicated by~~After the addition of inorganic nutrients~~t~~ addition, delays in bloom formation, the Δ TA gradient, indicated by the ~~g~~Gross ~~p~~Production (GP), ~~and n~~Net ~~c~~Community ~~p~~Production (NCP), ~~and the rates, as well as by the~~ chlorophyll-*a* (Chl_a) concentrations. Notably, the delay was more pronounced for the calcium treatment set compared to the silicate one, with ~~the~~ low TA treatments exhibiting earlier responses than ~~the~~ high TA ones. This delay is likely due to the previously documented species-specific negative relationships between high pH/low ~~p~~ CO_2 ~~levels conditions~~ and phytoplankton growth rates. This study underscores the need for further investigation into the implications of the ~~these~~ response patterns in terms of trophic transfer and seasonal ~~suitability~~ ~~timings~~ ~~suitability~~. ~~Further,~~ ~~Moreover,~~ it is anticipated that a ~~wider-greater~~ delay in bloom formation would be evident with a larger non-equilibrated TA gradient. ~~Thus,~~ highlighting the importance of exploring variations in TA ~~limits~~ ~~thresholds~~ for a comprehensive understanding of the OAE's impacts.

Keywords. OAE, alkalinization, silicate-based, calcium-based, community production, metabolic rates

1. ~~Introduction~~INTRODUCTION

To reduce the concentration of atmospheric carbon dioxide (CO_2), and to be able to stay below the 1.5 to 2 °C global mean temperature increase relative to preindustrial times, the realistic

emissions cut alone is projected not to be sufficient (Friedlingstein et al., 2022, 2019; Fuss et al., 2020; ~~IPCC, 2018, 2023~~; Lee et al., 2021). The changes to our technological and socio-economic systems that would be necessary to attain the required emissions reductions can take decades, or
40 longer, to be implemented (Renforth and Henderson, 2017). In fact, all the projections that simulate the agreed upon conditional and unconditional Nationally Determined Contributions (NDCs) in terms of emissions cuts, and that also assume gross negative emissions, still fall well above those in which the temperature is restricted to the targeted maximum increase (IPCC, 2023). The latter require more extensive emissions reductions, alongside reaching net-zero emissions by
45 2050, and net negative emissions for the rest of the century (~~IPCC, 2018, 2022~~) (O'Neill et al., 2016; Rogelj et al., 2018). Therefore, the need for atmospheric carbon removal and sequestration is imperative to avoid the serious, long-term climatic consequences associated with surpassing the aforementioned temperature limit, which is considered a tipping point.

Ocean alkalinity enhancement (OAE) is a marine carbon dioxide removal (mCDR) approach that
50 shows great promise. Model studies indicate that OAE shows the potential to remove atmospheric carbon ~~at-on~~ a gigaton (Gt) scale (Feng et al., 2017; Harvey, 2008). ~~A,~~ although it not only shows potential for carbon capture and long-term sequestration. It is also known to possibly aid in the alleviation of ocean acidification (OA; Albright et al., 2016; Gattuso et al., 2018; Feng et al., 2017; Harvey, 2008). OAE is attained through the addition, in various ways, of alkali or alkaline
55 compounds to seawater increasing total alkalinity (TA), pushing the carbonate equilibrium system from CO₂ to the bicarbonate (HCO₃⁻) and carbonate (CO₃⁻²) species (Kheshgi, 1995). This process allows for additional CO₂ diffusion in the course of regaining balance with the atmosphere and alleviates the effects of OA by increasing the ocean's buffering capacity.

CO₂ equilibration can be induced prior to the alkalinity addition, or the alkalinity plume can be
60 left to equilibrate naturally through sea-gas exchange, which is more feasible. Indeed, large scale equilibrated OAE application would require the use of reactors to CO₂ equilibrate the alkaline solutions before deployment (Hartmann et al., 2023). If left to natural sea-gas exchange, however, this process can take several months to years (Jones et al., 2014). Notably, when carbon dioxide is not chemically pre-sequestered, the alterations to the carbonate system become more
65 prominent. These consist of a substantial decrease in CO₂ partial pressure (~~pCO₂ pCO₂~~) and a subsequent significant increase in pH, particularly when compared to methods involving pre-equilibration. Such reduced ~~pCO₂ pCO₂~~-resulting from the alkalinity manipulation without prior equilibration could potentially lead to CO₂ limitation among phytoplankton (Riebesell et al., 1993).

70 Past studies have in fact reported taxon-specific responses in phytoplankton growth based on the combined effects of ~~pCO₂ pCO₂~~ and H⁺ concentration in the context of OA (e.g., Paul & Bach, 2020). Before OA became a central focus of scientific research, high pH/low CO₂ conditions were

observed to cause declines in marine phytoplankton growth rates (Goldman, 1999; Hansen, 2002). Notably, under air-equilibrated conditions, species-specific half saturation values ($k_{1/2}$) for HCO_3^- and CO_2 acquisition in photosynthesis have also been reported (Raven and Johnston, 1991). Hence, given that the utilization of non-equilibrated OAE will entail significant changes to ~~said~~ these carbonate system parameters ($p\text{CO}_2$ and H^+), a response in terms of microbial production rates in relation to the deployed non-equilibrated alkalinity gradient was expected.

Another factor of uncertainty when considering OAE implementation is the source mineral type, whether it is calcium or silicate based. For silicate-based OAE ~~deployment~~, naturally occurring olivine-rich minerals, such as dunite, ~~which contain forsterite (Mg_2SiO_4)~~, are being considered (Montserrat et al., 2017; Renforth and Henderson, 2017). ~~This This~~ is because olivine occurs commonly in nature and weathers relatively quickly, eliminating the need for energy-intensive chemical processing prior to dissolution (Renforth and Henderson, 2017; Schuling and Krijgsman, 2006). However, ~~olivine is comprised of forsterite (Mg_2SiO_4) and fayalite (Fe_2SiO_4) in a 9:1 ratio. An iron (Fe) addition may have a fertilizing effect on phytoplankton in the photic zone~~ (Bach et al., 2019a; Hauck et al., 2016; Renforth and Henderson, 2017), and it is the Mg end member of olivine that, as it weathers, consumes atmospheric CO_2 naturally (Köhler et al., 2013; Renforth and Henderson, 2017). Additionally, ~~its~~ olivine dissolution releases silicon, which may benefit silicifying plankton species ~~iers~~ (Bach et al., 2019a; Hauck et al., 2016), ~~(such as diatoms), and iron, which is a co-limiting micronutrient~~, but also other potentially harmful by-products such as nickel (Xin et al., 2023), and other trace metals (Bach et al., 2019a).

A calcium-based mineral that is being considered for OAE deployment is hydrated lime (Ca(OH)_2 ; Kheshgi, 1995). It is produced through the calcination of limestone and would dissolve much faster than any natural mineral (Renforth and Henderson, 2017). Besides, the latter does not contain any dissolution by-products that could in theory negatively impact biota. However, the introduction of calcium to the system may promote calcification (Albright et al., 2016; Bach et al., 2019a), a process through which CO_2 is emitted (Zeebe and Wolf-Gladrow, 2001). Thus, that would entail a reduction in the OAE's carbon capture efficiency, alongside benefiting benthic (Albright et al., 2016) and potentially pelagic calcifiers, so possibly also inducing a plankton community composition shift away from silicifiers (Bach et al., 2019a).

Considering all these ~~aforementioned unknowns~~ unknowns, the current study aimed at monitoring the response of the microbial community to a silicate versus a calcium-based, non- CO_2 equilibrated OAE implementation. To isolate the effects of the carbonate chemistry alterations in both case scenarios, and to avoid confounding variables due to impurities in the raw minerals, simulations of a forsterite (Mg_2SiO_4) and a hydrated lime (Ca(OH)_2) addition were employed. Compounds that ~~separately~~ contain the ~~mentioned~~ key elements present in ~~hydrated lime and forsterite~~ them separately, already in solution, were used. Gross and net oxygen production rates

(GP and NCP respectively), community respiration (CR) rates, metabolic balance (GP:CR), and chlorophyll *a* (Chl_a) concentration were monitored over a ~~10-week~~ 53-day period. Alterations driven by the mineral type, and the carbonate chemistry changes to these metabolic ~~mentioned~~ rates were expected (Bach et al., 2019a; Paul and Bach, 2020; Riebesell et al., 1993). Addressing the ~~aforementioned~~ knowledge gaps explained above is key in understanding the non-equilibrated OAE's environmental impacts, its potential for CO₂ removal in terms of efficiency and long-term sequestration, and thus in choosing a suitable approach for its safe deployment.

2. MATERIALS AND METHODS

2.1 Experimental setup and sampling

The experiment (KOSMOS Bergen 2022) was carried out in Raunefjorden, 1.5 km offshore from the Espegrend Marine Research Field Station, of the University of Bergen, Norway, under post-bloom conditions, starting on the 7th of May 2022. This location provided protection from swells and access to all the necessary facilities to conduct the experiment right onshore (Ferderer et al., 2023). Ten KOSMOS (Kiel Offshore Mesocosms for Ocean Simulations; Riebesell et al., 2013) units, or mesocosms, of an approximately 60 m³ capacity were deployed. The mesocosm cylindrical bags (20 m long and 2.5 m in diameter) were left submerged and opened at the bottom for approximately a week prior to the start of the experiment on the 13th of May. Therefore, allowing for enough open water exchange to enclose a natural planktonic community as homogeneously as possible amongst all mesocosms. To close them, the sediment traps (2 m long, funnel shaped) were placed on the bottom ends, the tops of the bags were drawn out 1m off the water's surface, and the mesocosm roofs were put in place. In order to exclude all unevenly allocated large organisms, a ring with the same diameter as the mesocosms (Riebesell et al., 2013), and with a 1 mm net attached to it, was pulled from bottom to top, just after mesocosm closure (Day 0). Two days after closure, the volume contained in the mesocosms was determined. To do that, the water inside the mesocosms was first homogenized using a spider-like dispensing device (named henceforth "spider", see Riebesell et al., 2013) to bubble compressed air up and down the water column. Later, by measuring salinity before and after adding 50 L of a precisely calibrated NaCl brine solution, also using the spider, ~~with a known concentration, and measuring salinity before and after said addition~~, the volume contained in each mesocosm could be calculated, as in Czerny et al. (2013). Mesocosm inside and outside cleaning was carried out once a week. Outside cleaning was done by divers and people assisting from boats, using brushes. The inside cleaning was realized sinking a ring with the same diameter as the mesocosms, with rubber blades around its circumference, and pulling it up. This way removing any growth found in the mesocosm walls that could interfere with the results of the experiment.

145 Samples from the entire 20 m water column inside the mesocosms, and from the fjord, were collected every two days using Integrated Water Samplers (IWS III, HYDRO-BIOS Apparatebau GmbH, Altenholz, Germany) with a 5 L internal volume capacity. Mesocosms were sampled in a random order and an extra sample from the fjord was always taken from the same location right next to mesocosms 5. After three sampling days (day 6), to properly monitor the starting conditions, the TA manipulation was applied. The experiment ended on the 6th of July, lasting 53
150 days. For further information on all the research and maintenance activities carried out throughout the experimental period, please refer to Supp. Fig. S1.

2.2 Carbonate chemistry manipulation and nutrient fertilization

The mesocosms were divided into two sets of five (see Table 1). ~~Out of one of these sets, four~~
155 ~~Five~~ mesocosms were treated with $\text{CaCl}_2 \cdot \text{H}_2\text{O}$, and with NaOH (Merck) setting a total alkalinity (TA) gradient from ΔTA 0, in increments of $150 \mu\text{mol} \cdot \text{L}^{-1}$, up to a ΔTA of $600 \mu\text{mol} \cdot \text{L}^{-1}$. The other set of five were treated with $\text{MgCl}_2 \cdot 6 \text{H}_2\text{O}$, $\text{Na}_2\text{SiO}_3 \cdot 5 \text{H}_2\text{O}$, and with NaOH (Merck) following the ~~said same~~ TA gradient. The amounts of Mg^{2+} and Ca^{2+} were increased in proportion to the NaOH addition, whereas the amount of Na_2SiO_3 added was the same ($75 \mu\text{mol} \cdot \text{L}^{-1}$ target concentration) in all the silicate based OAE treatments, including the control. The TA increase of
160 2:1 with respect to the amount of Na_2SiO_3 added was taken into consideration by reducing the amount of NaOH accordingly, and by adding diluted HCl in the silicate-based control (Ferderer, et al., 2023). The target amounts of NaOH, Na_2SiO_3 and MgCl_2 , and CaCl_2 for each treatment were dissolved in 20 L of MiliQ water. These were later added to the mesocosms, evenly up and down the water column, using the spider.

165 An inorganic nutrient addition was carried out on day 26 due to the oligotrophic conditions found inside the mesocosms compared to those observed in the fjord. But also, because the community inside was close to reaching heterotrophic balance even though the light conditions were reasonably optimal. The nitrate (NO_3^-) target concentration was set at $4 \mu\text{mol L}^{-1}$ to simulate a mixing event that would promote a phytoplankton boom comparable in biomass to natural
170 occurrences in the area. Phosphate (PO_4^{3-}) was added following the N:P Redfield ratio of 16:1 across all mesocosms, and silicate was added in an ~~N:Si:N~~ ratio of 1:44:1 only ~~in to~~ the calcium treatments. This ratio was chosen to provide a niche for coccolithophores, preventing them from being outcompeted by diatoms, which would be silicate limited under these conditions (Gilpin et al., 2004; Schulz et al., 2017). Further, this design choice ensured that the Si content in the Ca
175 treatments remained reasonably low, preserving the integrity of the mineral treatment differentiation, plus it roughly mirrored the silicate concentration in the fjord at the time. A second addition on day 28 was undertaken to correct for stoichiometric differences between mesocosms (see Ferderer, et al., 2023).

2.2 Carbonate chemistry

180 Samples for TA, ~~d~~Dissolved ~~i~~norganic ~~c~~Carbon (DIC), and total seawater pH were collected into 250 mL glass flasks, allowing for plenty overflow, directly from the IWSs. TA and pH samples were collected every two days, whereas DIC was only measured on day 9. Samples were later sterile filtered (~~25mm, 0.2~~ μm ~~PES membrane, syringe filters;~~ Filtropur S, SARSTEDT, Nümbrecht, Germany) with a peristaltic pump and with special care to avoid sea-gas exchange.

185 TA concentrations were determined by a potentiometric two step titration using a Metrohm 862 Compact Titrosampler with HCl 0.05 M as the titrant, an Aquatrode Plus (Pt1000), and a 907 Titrand unit, as in Chen et al., 2022. DIC concentrations were measured with an AIRICA system (Marianda, Kiel, Germany; see Gafar & Schulz, 2018, and Taucher et al., 2017) with a differential gas analyzer (LI-7000, LI-COR Biosciences GmbH, Bad Homburg, Germany) at room

190 temperature and within 12 h. Also, total seawater pH samples were acclimated to 25°C in a thermostatic bath and later measured spectrophotometrically, at the same temperature, with a VARIAN Cary 100 in a 10 cm cuvette (Dickson et al., 2007). The rest of the carbonate system parameters were calculated with CO2Sys v2.5 (Lewis and Wallace, 1998) using the measured TA, total seawater pH, and nutrient concentrations, as well as the in-situ temperature and salinity daily

195 means obtained from the CTD casts (see Sup. Fig. S1). pH was corrected against the measured DIC on day 9 (see Schulz et al., 2023).

2.3 Dissolved inorganic nutrient concentrations

Triplicate samples to account for technical variability were collected every two days. These were sterile filtered using 33mm, -0.45 μm PES membrane ~~-fiber~~ syringe filters (Filtropur S, SARSTEDT, Nümbrecht, Germany) and kept in the dark and at ambient temperature until ~~further~~ processing/analysis. Nitrate (NO_3^-), nitrite (NO_2^-), phosphate (PO_4^{3-}), and silicate ($\text{Si}(\text{OH})_4$) concentrations were determined spectrophotometrically as in Hansen & Koroleff (1999). Ammonia (NH_4^{\pm}) was measured using a 10-AU Fluorometer (TURNER designs, San Jose, CA, USA) following Holmes et al. (1999).

205 2.4 Metabolic rates through oxygen production and consumption

Gross ~~p~~Production (GP), ~~n~~Net ~~c~~Community ~~p~~Production (NCP), and ~~c~~Community ~~r~~Respiration (CR) rates were determined by oxygen production and consumption in calibrated 125 mL nominal volume soda lime glass bottles following the Winkler method and the recommendations from Carpenter (1966), Bryan et al. (1976), and Grasshof et al. (1999), also described by Marín-Samper et al. (2024). Polycarbonate bottles were filled with 4.5 L of seawater per mesocosm, and from the fjord on each sampling day directly from the IWSs and brought to the lab. Out of each 4.5 L sample, ten soda lime bottles were first rinsed with sample water and then randomly filled, allowing ample overflow, using a silicone tube with an attached 280 μm mesh on one end. Four

215 out of the ten subsamples per mesocosm were fixed ~~at the moment of right after~~ collection, “initials”, through the addition of 1 mL of a manganese chloride (MnCl₂) solution, and 1 mL of a sodium iodide (NaI) based alkaline solution, in this order. They were later covered with an ~~blackout-opaque~~ piece of fabric and stored upright in a rack underwater. Another three bottles were incubated inside opaque bags, namely “dark” ones, and the remaining three were incubated under “light” conditions. The latter were randomly distributed inside clear methacrylate
 220 incubators set outside, which were covered with a blue foil (172 Lagoon Blue foil, Lee filters, Burbank, USA) to better simulate the light spectrum of the water column, along with the “initials” ~~(already fixed and left upright to allow for the Mn(OH)₂ precipitate to settle)~~, and the bags containing the “dark” ones. The incubators were hooked to a constant water flow system that siphoned water directly out of the fjord (from 14 m depth), into the incubator, and out into the
 225 fjord again. Data loggers (HOBO UA-002-64, Australia/New Zealand) were placed inside the incubators to monitor the temperature (roughly 11.11 and 10.34 °C in average during the day and night, respectively) and light (ranging from 0.20 to 688.89 μmol photons m⁻² s⁻¹) conditions throughout the experiment. After an incubation period of 24 hours, all samples were fixed and left to sediment for at least 2 hours. Finally, samples were acidified with 1 mL of 5 M sulphuric acid
 230 (H₂SO₄) and analysed with an automated titration system, with colorimetric end-point detection (Dissolved Oxygen Analyzer, SIS Schwentinental, Germany), using a 0.25 M sodium thiosulphate solution (Na₂S₂O₃ * 5H₂O) as the titrant. The mean of each set of replicates was used to calculate CR, NCP, and GP rates, using the following Eq. (1), Eq. (2) and Eq. (3) respectively:

$$\text{CR} [\mu\text{mol L}^{-1}\text{h}^{-1}] = \frac{\text{Conc}_I - \text{Conc}_D}{h_D} \quad (1)$$

$$\text{NCP} [\mu\text{mol L}^{-1}\text{h}^{-1}] = \frac{\text{Conc}_L - \text{Conc}_I}{h_L} \quad (2)$$

$$\text{GP} [\mu\text{mol L}^{-1}\text{h}^{-1}] = \text{CR} + \text{NCP} \quad (3)$$

240 where Conc_I, Conc_D and Conc_L correspond to the mean oxygen concentration of the initial, dark, and light samples, respectively, ~~and h_L and h_D - F~~ stands for the light and dark samples' incubation time in hours. The metabolic balance was later calculated by dividing the obtained GP rates by the CR rates.

Due to a COVID outbreak in the base, the two scientists in charge of measuring this parameter had to be confined. Therefore, data were not collected on days 47 and 49.

2.5 Chlorophyll *a* concentration

245 Chlorophyll *a* (Chl*a*) samples for each mesocosm were collected into 500 - 1000 mL dark bottles from 10L canisters that were filled directly from the IWSs. Samples were filtered ~~through a 200 μm mesh~~ onto glass fiber filters (Whatman grade GF/F, 0.7 μm nominal pore size), with minimal

light exposure. Filters were stored in plastic vials at -80 °C and analyzed. Chl~~a~~ concentration was determined fluorometrically after Welschmeyer (1994) ~~the following day.~~

2.7 Data analysis

Data for days 47 and 49 for GP were calculated using the equation from a Spearman correlation model with Chl~~a~~, with both variables transformed to base-10 logarithm (Supp. Fig. S2). NCP rates for those two days were calculated using the equation obtained through also a Spearman correlation model of NCP with GP (Supp. Fig. S2). The calculated NCP was then subtracted ~~to~~ from the estimated GP to obtain the CR values for those two days. Daily linear regressions in relation to the target Δ TA were carried out to determine the evolution of the TA effect on the GP production and respiration-CR rates, and on the Chl~~a~~ concentration, on the metabolic balance (GP:CR) and on the assimilation numbers (GP:Chl~~a~~) observed. To aid in the system's response interpretation, the experiment was divided into two phases: pre-nutrient addition phase (phase I: from day 7 to day 25), and a post-nutrient addition phase (phase II: from day 27 to day 53).

3. RESULTS

3.1 Carbonate chemistry and inorganic nutrient concentrations

There were minor discrepancies between the target TA gradient concentrations and those actually ~~was~~ achieved. As the gradient increased, the differences between the expected and the attained TA concentrations widened, albeit with small differences between the silicate and calcium-based OAE treatments. The attained TA gradient was lower than the targeted levels, and, moving up said gradient, the mentioned observed differences slightly widened (Table 1). Additionally, no significant differences were observed between the meant to be equivalent, calcium and silicate-based treatments in Δ TA, and thus also in $p\text{CO}_2$, $p\text{CO}_2$ and pH either, were marginally distinct between the meant to be equivalent, calcium and silicate-based treatments, particularly in the three highest ones (Figure 1).

Table 1. The first column corresponds to the mesocosms (MK), and next to it the source mineral type. The target Δ Total Alkalinity (TA) gradient, in $\mu\text{molEq} \cdot \text{L}^{-1}$, is listed for each MK, with the measured or "attained" mean Δ TA, and finally the difference between the theoretical/target gradient and the actual mean Δ TA obtained.

MK	Mineral	Target Δ TA	Attained Δ TA	Target-Attained
M5	Ca	0	0	0
M1	Ca	150	138.4	11.6
M9	Ca	300	287.5	12.5
M7	Ca	450	404.0	46.0
M3	Ca	600	530.0	70.0
M6	Si	0	0	0
M10	Si	150	140.3	9.7
M2	Si	300	278.9	21.1

M4	Si	450	422.4	27.6
M8	Si	600	550.4	49.6

The mean pH levels ~~obtained~~ ranged from 8.06 ± 0.02 to 8.71 ± 0.03 , and from 8.03 ± 0.02 to 8.72 ± 0.02 , in the calcium and silicate treatments respectively (Figure 1 B). In terms of mean $p\text{CO}_2$, the difference between the controls and the highest treatments was ~~quite steep~~ substantial, going from 372.3 ± 19.7 and 397.05 ± 20.4 μatm , in the calcium and silicate controls, down to 76.08 ± 7.4 and 72.6 ± 5.07 μatm in the highest treatments, correspondingly (Figure 1 C).

A noteworthy result is that full natural equilibration did not occur after a 53-day long experiment. CO_2 incursion was minor, as it is clear from the relative stable pH and $p\text{CO}_2$ -levels observed in the treated mesocosms during the whole experiment (~~included in~~ Figure 1 B and C). In fact, when deducting the calculated $p\text{CO}_2$ -levels obtained on day 53, to those observed right after the TA manipulation on day 7, ~~differences fall between~~ $p\text{CO}_2$ increased between 75.98 and 12.75 μatm increased between 63.9 and 12.75 μatm in the treated mesocosm. Additionally The gap in absolute $p\text{CO}_2$ values being h, ~~the higher increases in absolute $p\text{CO}_2$ values were observed in the low~~, and follow a declining gradient going from the $\Delta\text{TA} \theta$ -treatments and declining towards high following the ΔTA gradient mesocosm to the highest ones (Supp. Table S1). Nevertheless, percentage enhancements were similar among same treatment mesocosms, $36.80 \pm 2.60\%$ and $27.07 \pm 6.22\%$ in Ca and Si based treatments, respectively. Controls presented the highest absolute increase in $p\text{CO}_2$ 75.98 yet the lowest percentage, $17.16 \pm 7.16\%$. Therefore, ~~the neither the pH nor the and $p\text{CO}_2$ -levels in the mesocosms where TA was manipulated never did not reached, nor got closer to, the ambient levels throughout the experiment. observed in the "controls".~~

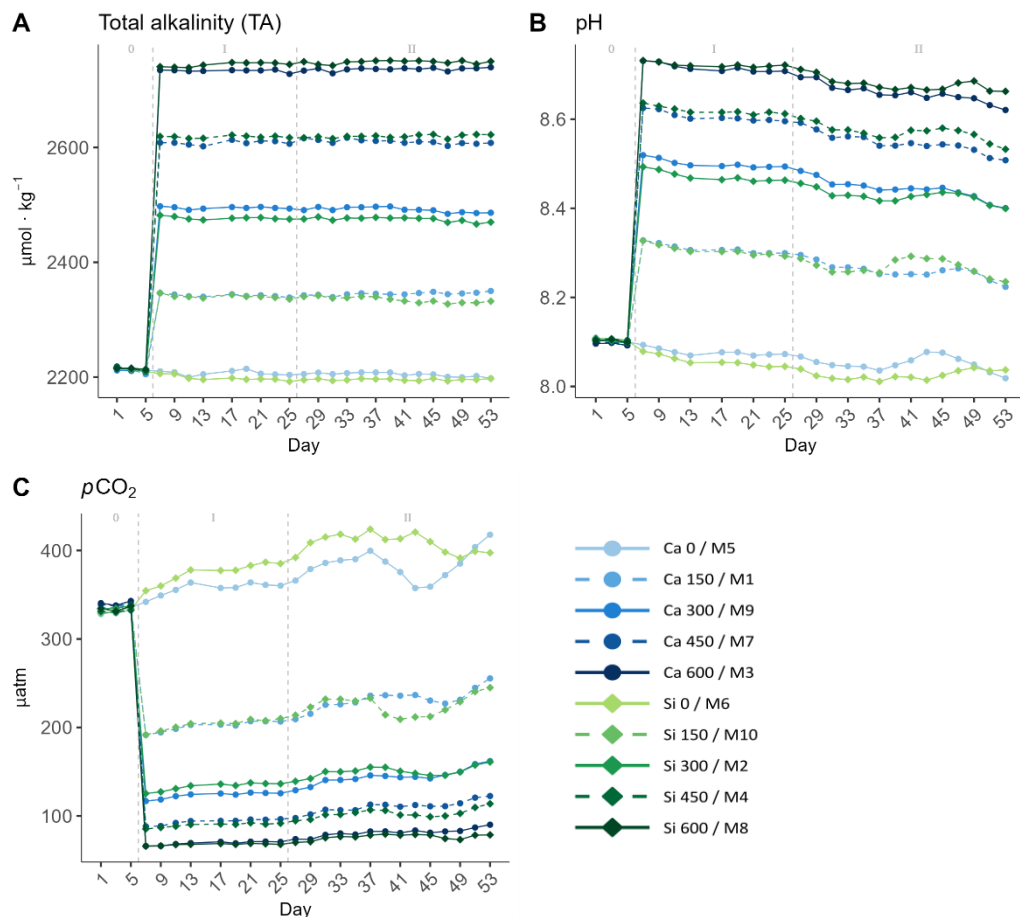


Figure 1. Temporal development of A) Total Alkalinity (TA), B) pH and C) partial pressure of CO_2 ($p\text{CO}_2$) attained throughout the experiment. In the legend, the blue gradient corresponds to the Calcium (Ca) treatments, and the green gradient to the Silicate (Si) based ones, in both cases followed by the target delta TA levels. The grey dotted lines in all the graphs mark the (left) TA addition on day 6 and the (right) nutrient fertilization on day 26. The numbers at the top of each graph refer to the phases defined by these two additions.

Nutrient concentrations (Figure 2) were significantly low at the beginning of the experiment. Conditions at the beginning of the experiment were consistent with those typically observed in a post-bloom scenario, characterized by markedly low nutrient concentrations (Figure 2). In fact, all measured nutrients presented values that are characteristic of a post-bloom environment. In fact, nitrate (NO_3^-) concentrations were below or close to the detection limit during phase I. (The mean NO_3^- concentration between from day days 7 and 25 was $0.004 \pm 0.035 \mu\text{M}$), PO_4^{3-} with silicate ($\text{Si}(\text{OH})_4$), in the calcium treatments, ranged from 0 to $0.09 \mu\text{M}$, and $\text{Si}(\text{OH})_4$ in the calcium treatments, phosphate (PO_4^{3-} between 0.06 and $0.44 \mu\text{M}$) concentrations ranging from 0.06 to $0.44 \mu\text{M}$ and from 0 to $0.09 \mu\text{M}$, respectively. In contrast, The $\text{Si}(\text{OH})_4$ concentration in the silicate based treatments, also in phase I, ranged from 65.9 to $69.8 \mu\text{M}$. No $\text{Si}(\text{OH})_4$ uptake was observed during this phase. After the nutrient addition on day 26, that depicts the start of phase II, a second addition was carried out on day 28 to correct for stoichiometric differences between mesocosms (Supp. Fig. S1 and Figure 2). Mean $\text{Si}(\text{OH})_4$ (in the calcium treatments, no

further Si(OH)_4 was added in the silicate treatments), NO_3^- , and PO_4^{3-} concentrations after addition on day 28 were of 1.07 ± 0.06 , 3.62 ± 0.1 , and 0.2 ± 0.02 μM respectively.

The average concentrations of the three inorganic nutrients across the silicate and calcium treatments separately on day 29 and on the last day of the experiment, were calculated. The average concentrations for the last day were subtracted ~~to~~ from those obtained on day 29 for the two mineral treatments separately. In the calcium treatments, 1.03 ± 0.06 μM , 3.56 ± 0.09 μM and 0.19 ± 0.01 μM of Si(OH)_4 , NO_3^- , and PO_4^{3-} respectively, were consumed during phase II. In the silicate ones, the decrease in the average NO_3^- , and PO_4^{3-} concentrations observed across all treatments was highly similar (3.67 ± 0.09 μM and 0.19 ± 0.02 μM). However, a steeper decrease of 10.79 ± 1.5 μM of Si(OH)_4 , compared to that observed for the calcium treatments, was detected due to the increased availability. ~~Thus, suggesting the community was silicate limited in the calcium treatments, and nitrogen limited in the silicate ones.~~ Additionally, silicate uptake starts started to occur later in phase II in the calcium treatments than in the silicate ones. For further details on nutrients dynamics see Ferderer et al. (2023).

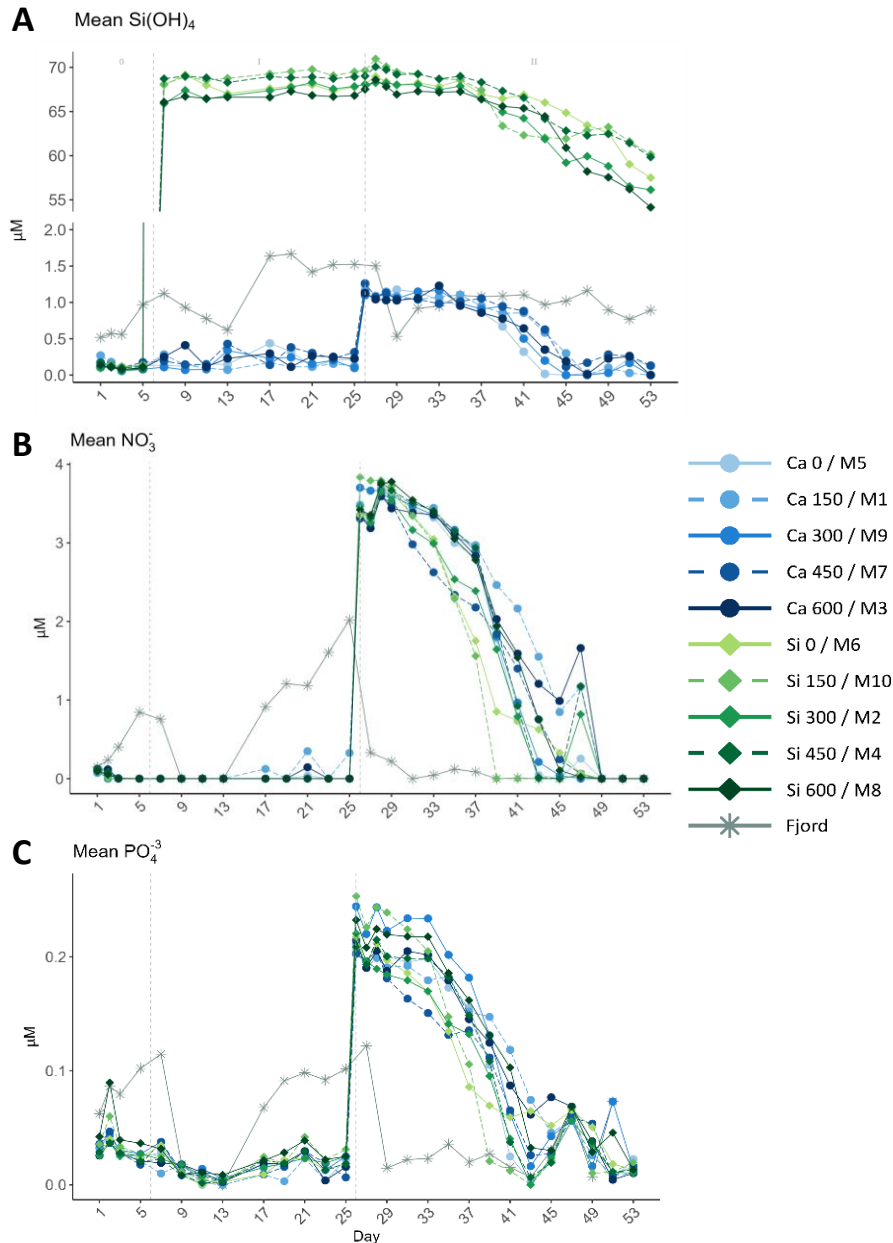


Figure 2. Temporal development of the mean A) silicate (Si(OH)_4), B) nitrate (NO_3^-) and C) phosphate (PO_4^{3-}) obtained from triplicate daily measurements throughout the experiment. In the legend, the blue gradient corresponds to the Ca treatments, and the green gradient to the Si based ones, in both cases followed by the target delta total alkalinity (TA) levels. The grey dotted lines in all the graphs mark the (left) TA addition on day 6 and the (right) nutrient fertilization on day 26. The numbers at the top of each graph refer to the phases defined by these two additions.

3.2 Metabolic rates and chlorophyll a concentration

After mesocosm enclosures, before the TA manipulation, mean GP₂ and CR and Chl a decreased by about half from rates were $5.31 \pm 0.8 \mu\text{mol O}_2 \cdot \text{L}^{-1} \cdot \text{d}^{-1}$, and $1.57 \pm 0.3 \mu\text{mol O}_2 \cdot \text{L}^{-1} \cdot \text{d}^{-1}$ and $1.08 \pm 0.2 \mu\text{g} \cdot \text{L}^{-1}$ on day 1, respectively, to $2.43 \pm 0.4 \mu\text{mol O}_2 \cdot \text{L}^{-1} \cdot \text{d}^{-1}$, and $0.58 \pm 0.08 \mu\text{g} \cdot \text{L}^{-1}$ on day 9, right after the TA addition, respectively and the mean Chl a concentration was $1.08 \pm 0.2 \mu\text{g} \cdot \text{L}^{-1}$ (Figure 3). A slight drop to half of the mentioned observed GP and Chl a , and almost half of the CR rates, was observed detected right after the addition in all treatments, down

340 to 2.43 ± 0.4 and $0.98 \pm 0.5 \mu\text{mol O}_2 \cdot \text{L}^{-1} \cdot \text{d}^{-1}$ on day 9 respectively (Figure 3). However, ~~n~~No significant ~~linear trends were~~TA effect was found in this short-term response phase, nor was there a difference between the two sets of mineral treatments (Figure 4). After a small rise during days 11-13, and in concordance with nutrient availability, both GP and Chl a continued to fall towards the end of the phase~~phase I on~~ By day 25,~~CR showed a similar pattern than GP and Chl a during~~ this phase. It decreased from $1.57 \pm 0.3 \mu\text{mol O}_2 \cdot \text{L}^{-1} \cdot \text{d}^{-1}$ on day 1, to $0.98 \pm 0.5 \mu\text{mol O}_2 \cdot \text{L}^{-1} \cdot \text{d}^{-1}$ on day 9, yet it recovered fully by day 13. Afterwards, CR rates decreased throughout the first phase and the beginning of the second, reaching values below $1 \mu\text{mol O}_2 \cdot \text{L}^{-1} \cdot \text{d}^{-1}$ on day 25-27~~CR accounted for over half of the GP,~~ that was at $2.02 \pm 0.5 \mu\text{mol O}_2 \cdot \text{L}^{-1} \cdot \text{d}^{-1}$, while in the Fjord, the GP rate reached a value of over $20 \mu\text{mol O}_2 \cdot \text{L}^{-1} \cdot \text{d}^{-1}$, and CR was slightly almost $2.5 \mu\text{mol O}_2 \cdot \text{L}^{-1} \cdot \text{d}^{-1}$. The same

345

350 A similar pattern as for the GP was observed for the Chl a concentration. CR rates recovered fully by day 13 and remained relatively constant ranging between little under~~slightly below 1, and 2 $\mu\text{mol O}_2 \cdot \text{L}^{-1} \cdot \text{d}^{-1}$ throughout this first phase.~~ In the second phase, and after the nutrient addition, GP rates and Chl a concentrations in the mesocosms increased, reaching maximum values between

355 days 37 and 47 (Figure 3 and 4). The~~A discrepancy between the treatments reaching the maximum values is~~ was striking noticed. It was observed that the low TA treatments responded to the nutrient addition slightly earlier than the high TA treatments, regardless of the ~~salt~~ compound added to each ~~set the~~ alkalinity gradient, i.e. Ca or Si (Figure 4 and S3). Low TA treatments not only responded earlier, but also reached higher GP and Chl a values (Figure 4 and S3). As a result, we observed a

360 progressive change in the direction of the daily linear ~~correlations~~ model slopes. When low TA treatments began to increase until they peaked (i.e., from day 31 to 37 in the silicate, and from day 37 to 41 in the calcium treatments) negative slopes were obtained (Figure 4, S4 and S5). Thereafter, due to the ~~decreased~~ decreasing productivity of in the low TA treatments and the increased ~~of~~ in the high ones, slopes progressively became positive reaching maximum values

365 on day 43 and 47 ~~when highest~~ the highest silicate and calcium-based TA treatments, M3 and 8 and 3 respectively, presented their maximum GP values (Figure 4, S4 and S5). ~~;~~

~~However~~Additionally, when comparing the production and Chl a ~~a~~ in the fjord and the mesocosms during the blooms, assimilation numbers (GP: Chl a) ~~were~~ were ~~inferred to be~~ much higher in the former than in the latter.

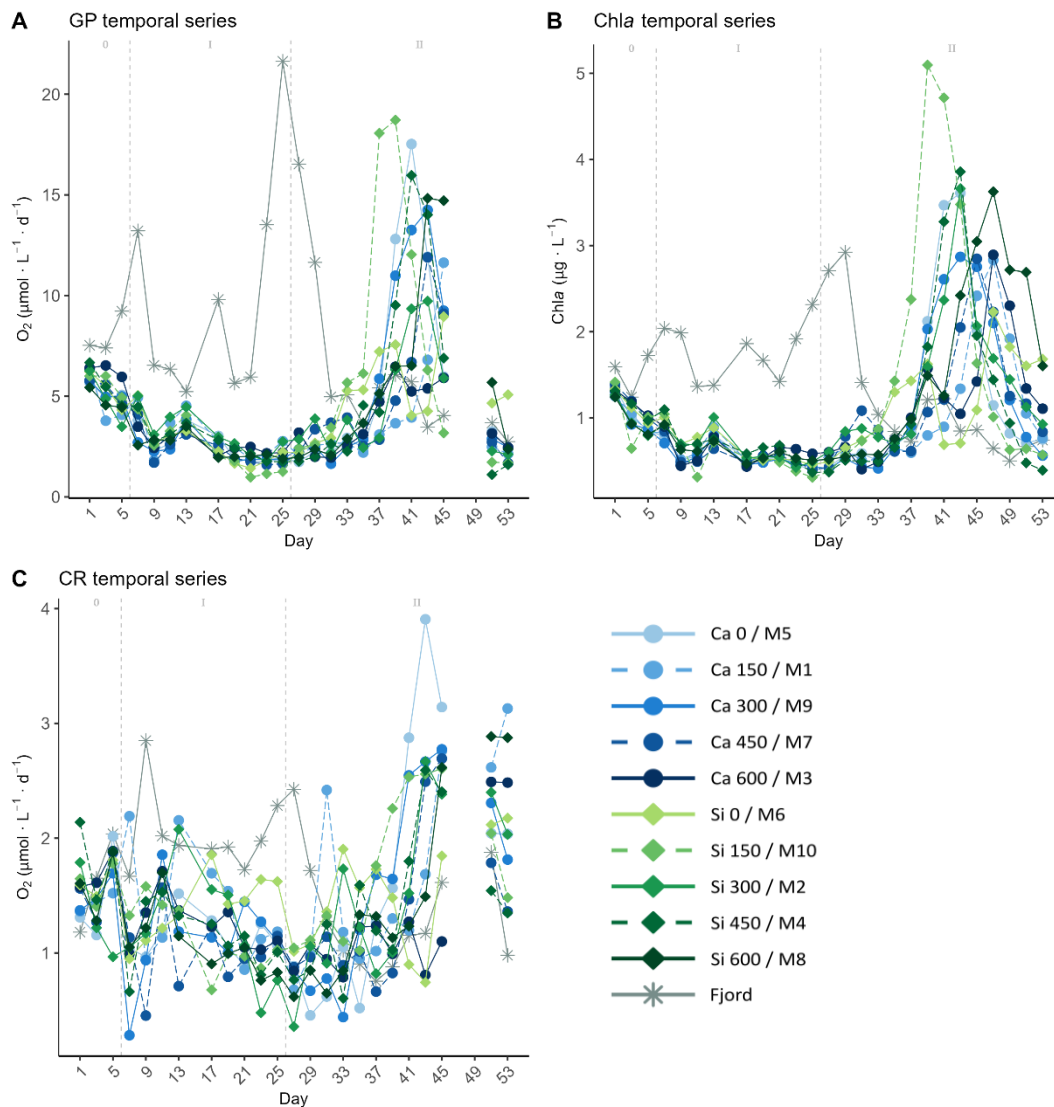


Figure 3. Temporal developments of the measured A) **g**Gross **p**roduction (GP), B) **ch**lorophyll **a** (Chla) concentrations and C) **c**ommunity **r**espiration (CR), throughout the experiment. In the legend, the blue gradient corresponds to the **c**alcium (Ca) treatments, and the green gradient to the **s**ilicate (Si) based ones, in both cases followed by the target delta **t**otal **a**lkalinity (TA) levels. **The grey dotted lines in all the graphs mark the (left) TA addition on day 6 and the (right) nutrient fertilization on day 26.** The numbers at the top of each graph refer to the phases defined by these two additions.

370

In the temporal series included in the previous figure, no apparent pattern can be discerned. However, when looking at these parameters over time for each mesocosm individually, as seen in Supp. Fig. S33, the low TA treatments are seen to respond to the nutrient addition slightly earlier than the high TA ones. This pattern is portrayed more clearly in Figure 4. The slopes \pm and 95 % confidence intervals obtained from daily linear models of GP and Chla with the Δ TA gradient (Supp. Fig. S4 and S5, respectively), as well as the absolute daily values, were plotted over time for the silicate and the calcium treatments separately.

375

Overall When comparing between salt mineral-based treatments, we observed that both GP rates (Figure 4 A and B) and Chla concentrations (Figure 4 C and D) were marginally higher in the silicate-based than in the calcium-based treatments (Figure 4 and S3). Additionally Furthermore,

380

as mentioned earlier, they responded slightly earlier to the nutrient addition in the silicate treatments both (Figure 4 A and C) augmented earlier than in the calcium ones. Indeed, the increase in GP in the silicate-based treatment with the highest TA coincided with the peak in GP in the calcium treatments with the lowest TA (Figure 4 and S3). This is supported by the trend in, for instance, Si(OH)_4 concentration's temporal development (Figure 2 A), but also by the fact that while negative slopes were observed for silicate treatments from day 31 on, they were not observed for the calcium set until day 37 (Figure 4, S4, and S5)., showing a negative slope with the ΔTA gradient starting on day 31, which peaked by day 37. Posteriorly, the low TA treatments began to drop, and the GP and $\text{Chl}a$ concentration in the high TA ones started to increase. Thus, the slope obtained from the mentioned daily linear models reversed, peaking on day 41. In contrast, in the calcium treatments (Figure 4 B and D), since the response in the control and low TA mesocosms began 3 sampling days later, the highest negative slope was observed on day 41. Meaning thus that Therefore, the increase in GP increase in the silicate based highest treatments corresponded coincided with when the peaks GP peaked in the low TA calcium ones occurred. Therefore Hence, portraying a the delay in the community's response to the nutrient addition that was longer for the calcium treatments than the silicate treatments, and in both cases that followed the TA gradient (Figure 3A and B).

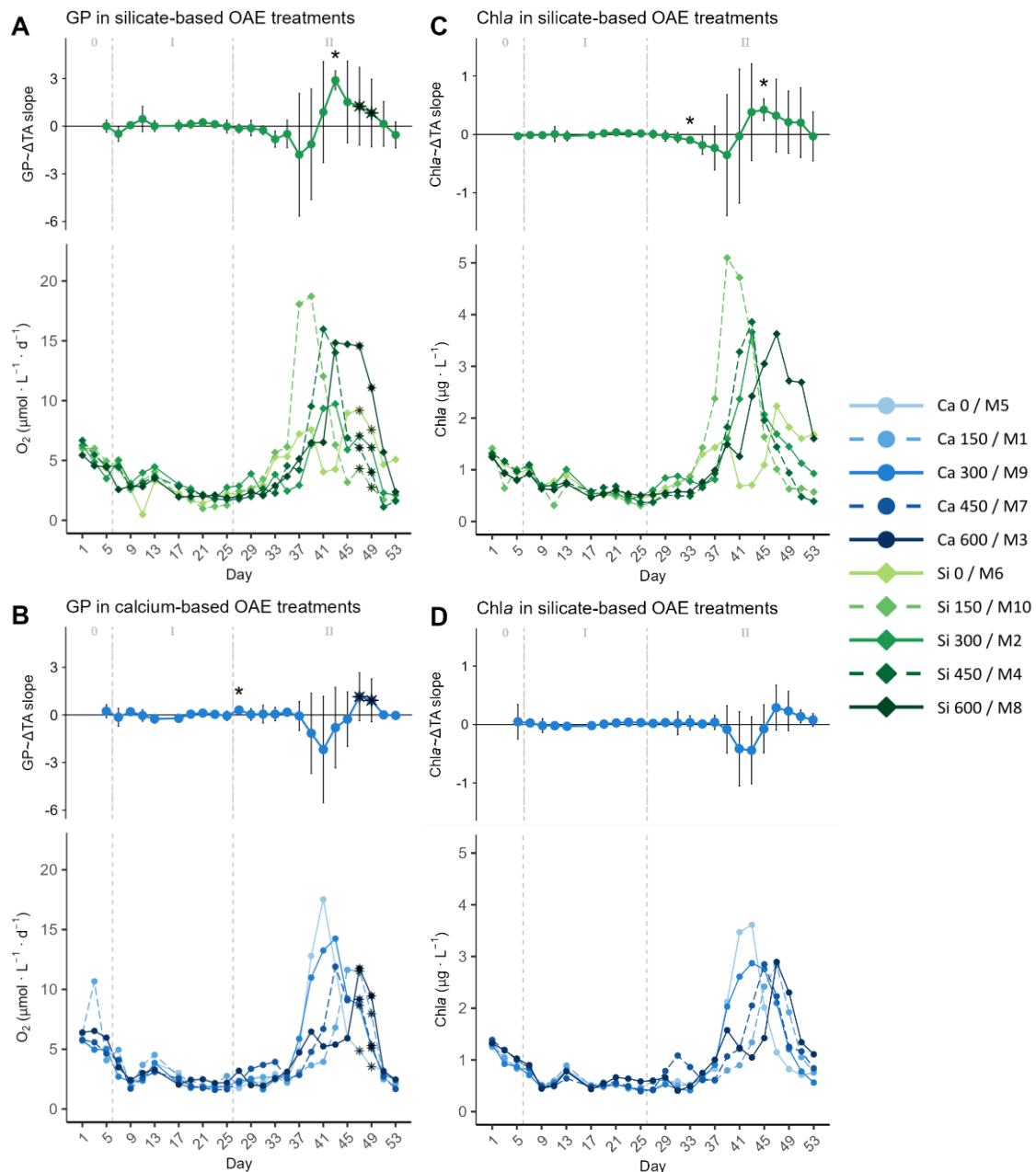


Figure 4. Temporal development of the (top under each letter) delta Δ Total Δ Alkalinity (TA) effect size (slope \pm 95% confidence intervals of daily linear models, [Figure S4 and S5](#)) on, and (bottom within each panel) absolute measurements of (A and B) Δ Gross Δ pProduction (GP) and (C and D) Δ Chlorophyll Δ *a* (Chla), separated by mineral treatment, where the silicate-based treatments are represented in A and C, and the calcium ones in B and D. The days when a significant relationship (p-values < 0.05) was observed are indicated with a star above the CI bars. The data points marked with a black star on top (days 47 and 49) were estimated by correlating the base-10 logarithm of GP and base-10 logarithm of Chla and using the spearman model equation to calculate the missing GP values ([Supp. Fig. S2](#)). In the legend, the blue gradient corresponds to the Δ Calcium (Ca) treatments, and the green gradient to the Δ Silicate (Si) based ones, in both cases followed by the target Δ TA levels. The grey dotted lines in all the graphs mark the (left) TA addition on day 6 and the (right) nutrient fertilization on day 26. The numbers at the top of the size effect graphs refer to the phases defined by these two additions.

Although samples for oxygen-based metabolic rates were not collected on days 47 and 49 due to the COVID outbreak, it was possible to obtain data for Chla, data for GP on days 47 and 49 could not be obtained. During these days, the Chla concentration in the high TA calcium treatments increased, inverting the relationship with the Δ TA gradient as in the silicate-based

400

treatments. The measured Chl_a concentrations were correlated with the GP rates and the model equation (Supp. Fig. S24) was used to calculate the missing GP data points. The calculated values are marked with black stars in the figures Figures 4A and B, and all that follow. To calculate the missing CR values, the measured GP and NCP rates were correlated, so that the missing NCP rates could be calculated with the latter model equation (Supp. Fig. S25), and then subtracted from the previously estimated GP. CR contributed significantly less than NCP to GP during the second phase.

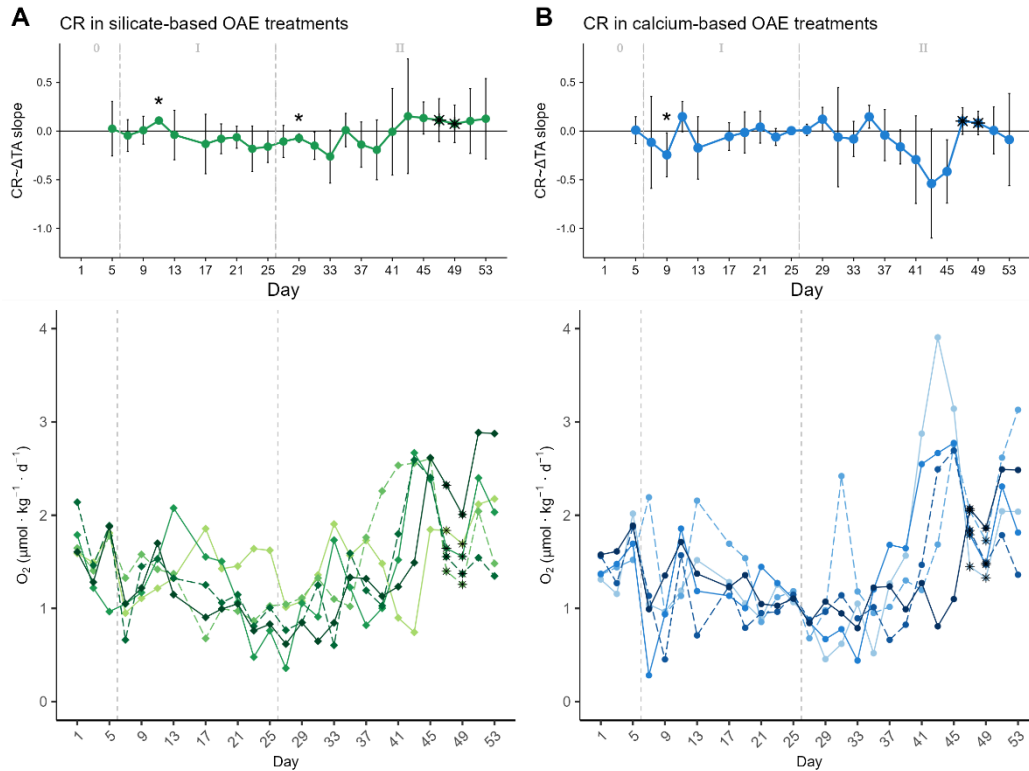


Figure 5. Temporal development of the delta Total Alkalinity (TA) effect size (slope \pm 95% confidence intervals of daily linear models, Figure S6) on, and (bottom within each panel) the temporal development of the absolute the Community Respiration (CR) rates for the (left) silicate and (right) calcium-based treatments. The days when a significant relationship (p-values < 0.05) was observed are indicated with a star above the CI bars. The data points marked with a black star on top (days 47 and 49) were estimated by correlating the measured Net Community Production (NCP) to the Gross Production (GP), then using the obtained Spearman model equation to calculate the missing NCP values, and finally subtracting the latter to the calculated GP values. These were estimated using the Spearman correlation equation of base-10 logarithm of the measured GP and base-10 logarithm of Chl_a. The vertical grey dotted lines in all the graphs mark the (left) TA addition on day 6 and the (right) nutrient fertilization on day 26. The numbers at the top of each graph refer to the phases defined by these two additions.

CR rates in the second phase. In the silicate treatments, CR did not portray the aforementioned pattern that was followed by the GP rates and the Chl_a concentrations described above (Figure 5A). They showed an increase after day 41, probably fueled by the organic matter produced during phytoplankton growth. Nonetheless, indeed, the progression from negative to positive slopes observed also for CR, as well as the earlier response of Si versus Ca-based treatments support the idea that high respiration rates were sustained by primary production at negative slopes obtained from daily linear models peaking on day 41 and that reversed on day 47, as

430 ~~observed in terms of GP and Chl a in the calcium treatments, was partially apparent can be partially
inferred in the CR rates observed in the calcium treatments (Figure 5B). The latter's CR in the
low TA calcium treatments portrayed an increased in CR around the same time as in terms of GP
and, the calculated CR rates that followed showed a slight recovery in the high TA treatments.~~

435 ~~Outside the mesocosms, in the fjord, conditions were the situation was very different. GP rates
and Chl a concentration remained close to the initial values, showing three peaks around days 7,
17, and 25, fueled by nutrient inputs (Figure 2). Of the three peaks, the last one was the most
intense reaching over 20 $\mu\text{mol O}_2 \cdot \text{L}^{-1} \text{d}^{-1}$, and up to 3 $\mu\text{g} \cdot \text{L}^{-1}$ of Chl a , respectively. This bloom
supposed the depletion of NO_3^- and PO_4^{3-} ~~NO_3^- and PO_4^{3-}~~ (Figure 2), and thus the collapse of the
bloom by day 33. Both GP and Chl a continued decreasing to values below initial conditions
towards the end of the experiment. A similar pattern was showed by CR in the fjord, with the last
440 peak reaching almost 2.5 $\mu\text{mol O}_2 \cdot \text{L}^{-1} \text{d}^{-1}$, yet no increase was observed on day 17. Furthermore,
CR values were of the same magnitude of the initial ones from the end of the bloom towards
the end of the experiment (Figure 3 C).~~

3.3 Metabolic balance and assimilation numbers

445 The absolute metabolic balance (GP:CR ratio) in both treatments presented a similar pattern trend
~~was mostly above 1~~ throughout the experiment (Figure 6). Values were consistently above 1
indicating that respiration was greater than production, i.e. Thus, meaning that overall, the
community was in an autotrophic state, even during phase I when low nutrient availability inside
of the mesocosm constrained primary the PP productivity. Due to nutrient starvation in the phase
I and the consequent decrease of in GP, Besides, particularly in phase II, the absolute metabolic
balance GP:CR presented its minimum on day 21-25. After the nutrient addition, GP:CR values
450 increased, reaching maximum values between days 33 and 45. Afterwards, GP declined but CR
was enhanced leading to a new decrease in GP:CR. It should be noted that in the last 2 days of
the experiment, GP:CR ratio presented values below 1, i.e., the systems became heterotrophic
after phase II blooms.

455 Overall, comparing both treatments, in overall, we observed was were observed to be slightly
higher values were observed in the silicate treatments when compared to the than in the calcium
ones, being more pronounced during bloom development in phase II. The between peak delay
pattern observed in GP and Chl a was only apparent for the silicate treatments (Figure 6 A).

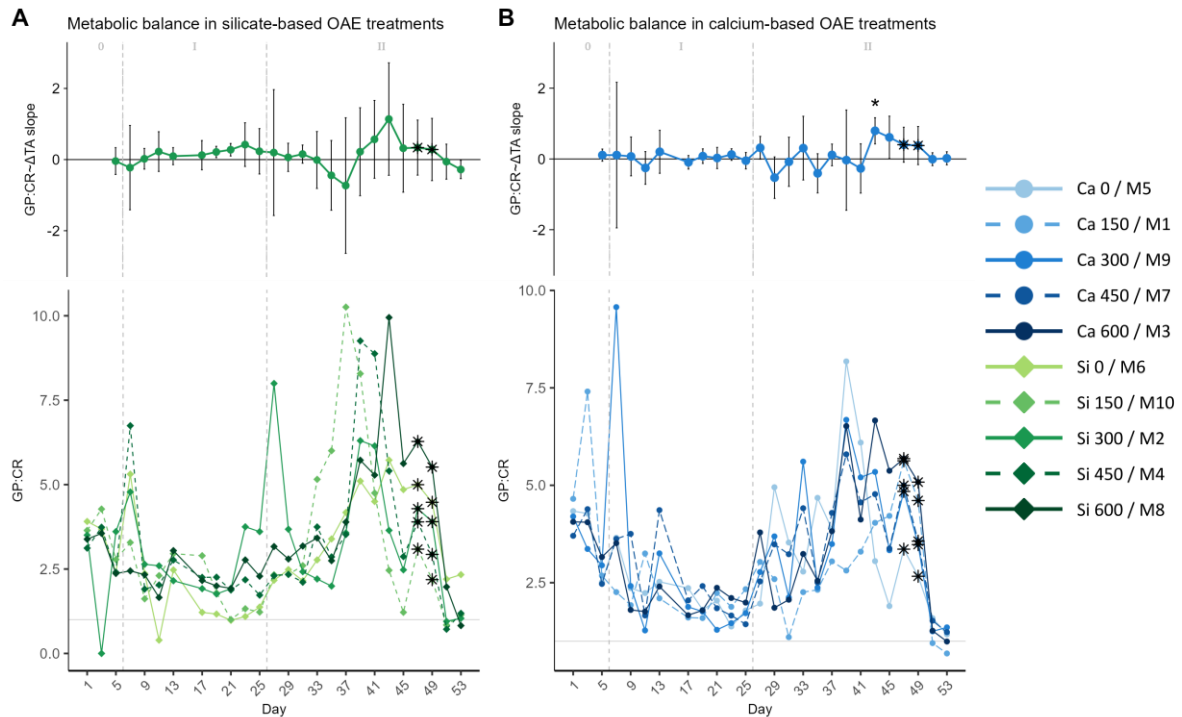


Figure 6. Temporal development of the (top under each letter) Δt -Total Alkalinity (TA) effect size (slope \pm 95% confidence intervals of daily linear models, [Figure S7](#)) on, and (bottom within each panel) of the calculated metabolic balance (ratio of ϵ Gross Pproduction, GP, over ϵ Community rRespiration, CR), where A) represents the silicate-based treatments, and B) the calcium ones. The days when a significant relationship (p -values $<$ 0.05) was observed are indicated with a star above the CI bars. The data points marked with a black star on top (days 47 and 49) were calculated by dividing estimations of GP and CR. The missing GP values were estimated using the spearman correlation equation of the base-10 logarithm of GP and base-10 logarithm of Chl a . Then CR were calculated by correlating the measured Net Community Production (NCP) to the Gross Production (GP), then using the obtained spearman model equation to calculate the missing NCP values, and finally subtracting the latter to the calculated GP values. In the legend, the blue gradient corresponds to the Calcium (Ca) treatments, and the green gradient to the Silicate (Si) based ones, in both cases followed by the target delta TA levels. The grey dotted lines in all the graphs mark the (left) TA addition on day 6 and the (right) nutrient fertilization on day 26. The numbers at the top of the size effect graphs refer to the phases defined by these two additions.

465 ~~When examining the overtime effect size of the Δ TA, the pattern observed for the Chl a and GP described above is only apparent for the metabolic balance GP:CR in the silicate treatments (Figure 6 A). Although, late in phase II, around the same time as for the silicate treatments, the latter parameter GP:CR in the high calcium treatments also increased with respect to the low TA ones (Figure 6 B). Additionally, in the silicate treatment set during phase I, and as is evident from the effect size graph in Figure 6 A, a mild positive effect of Δ TA is visible until the nutrient addition.~~

470 ~~Further, to see if the observed pattern also translated, to some extent, to the community composition of likely, the microphytoplankton fraction, assimilation numbers based on the GP rates were calculated. GP was chosen due to the low CR rates observed when compared to the~~

475 ~~NCP, especially during the second phase. Additionally, because when the NCP was positive, the~~

actual production that is occurring must be at least as much as the CR. The GP normalization using Chl_a as a biomass proxy (GP:Chl_a) yielded assimilation numbers that remained reasonably constant throughout the experiment and overall, unaffected neither by the mineral treatment, nor by the TA increment gradient (Figure 7). Differences between phases were not apparent either. In the fjord though, the assimilation numbers in the last bloom on day 25 reached a maximum that was higher than those observed in the mesocosms throughout phase II (see temporal series in Figure 7).

480

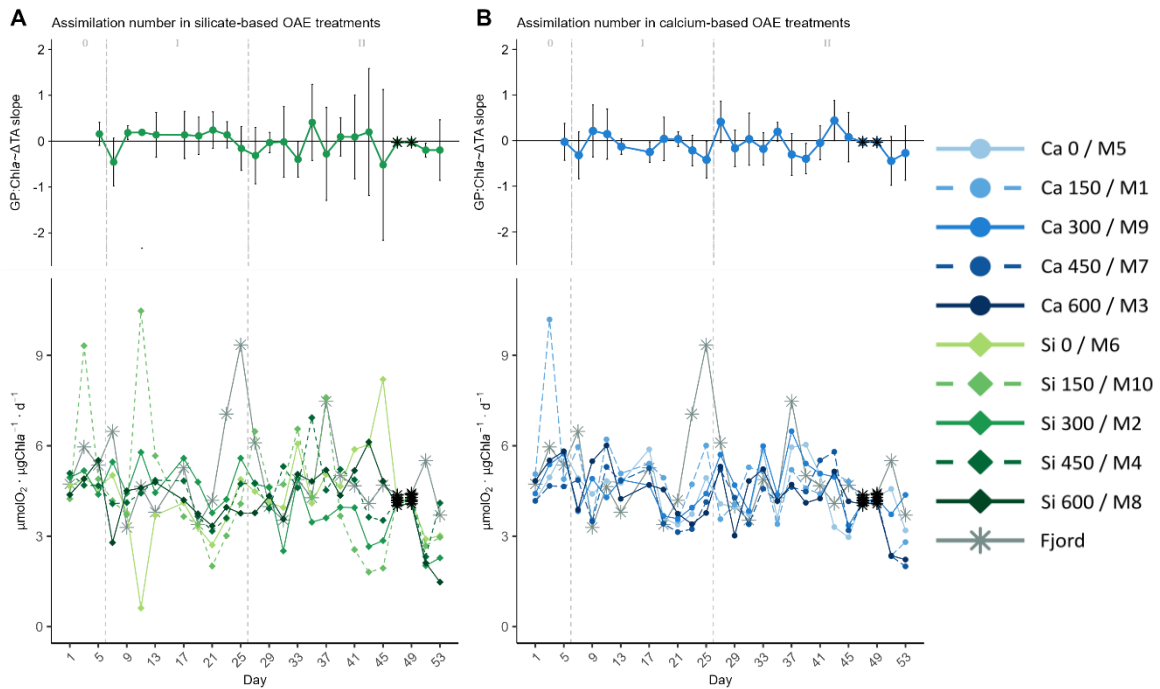


Figure 7. Temporal development of the (top under each letter) delta Total Alkalinity (TA) effect size (slope \pm 95% confidence intervals of daily linear models, Figure S8) on, and (bottom within each panel) of the calculated assimilation numbers (ratio of Gross Production, GP, over Chlorophyll *a*, Chl_a, concentration), where A) represents the silicate-based treatments, and B) the calcium ones. The data points marked with a black star on top (days 47 and 49) were calculated because GP could not be measured on those days. The missing GP values were estimated using the spearman correlation equation of the base-10 logarithm of GP and base-10 logarithm of Chl_a. In the legend, the blue gradient corresponds to the Calcium (Ca) treatments, and the green gradient to the Silicate (Si) based ones, in both cases followed by the target delta TA levels. The grey dotted lines in all the graphs mark the (left) TA addition on day 6 and the (right) nutrient fertilization on day 26. The numbers at the top of each graph refer to the phases defined by these two additions.

In all the previous Figures portraying the effect size of Δ TA over time, statistical significance (p value < 0.05) was indicated with a star on top (*) of the days when it was observed. The 95% confidence intervals are wide, suggesting high variability on individual days during phase II. The two treatments that deviate from the trend described in terms of GP and Chl_a are the control in the silicate treatment set, and the Δ 150 in the calcium one. The former portrayed two small peaks during the bloom phase and the highest CR rates right before the addition (Figure 5 A, bottom), and the latter the lowest GP:CR values in the second phase (Figure 6 B, bottom), and a longer delay than the control (Supp Fig. S4 and S5 respectively). Thus, due to the small sample size of

485

490

the mineral treatments (n = 5) on each individual day, these figures are used to portray the observed pattern more clearly. Not to summarize statistical outputs.

495 4. DISCUSSION

The experiment described herein involved the application of two distinct alkalinity gradients utilizing two ocean alkalinity enhancement (OAE) strategies based on different minerals: forsterite (Mg_2SiO_4) and hydrated lime ($Ca(OH)_2$). Forsterite is the Mg endmember of olivine, which occurs commonly in nature, while hydrated lime is produced through the calcination of limestone (Renforth and Henderson, 2017). Both minerals have been considered for OAE implementation; however, experimental studies on their potential impacts on natural communities remain unaddressed.
500 ~~The experiment presented here consisted of the deployment of two separate alkalinity gradients using two OAE strategies based on different minerals: hydrated lime and forsterite. The latter are both being considered for OAE implementation, but no experimental~~
505 ~~work on their potential effects on natural communities has been undertaken to date.~~ In the present current study, simulations were carried out by, instead of using the raw minerals, diluting the elements that conform them separately to reduce the potential effects of confounding variables such as the release of raw mineral impurities.

Large scale equilibrated OAE deployment would require the use of reactors for pre-equilibration (Hartmann et al., 2023) so it would be much more costly and less scalable, and thus less sealable and feasible. Therefore, CO_2 sequestration was not conducted prior to the alkalinity manipulation ~~in order~~ to evaluate the potential effects of the carbonate chemistry alterations associated with a non-equilibrated OAE deployment. These entailed a persistent increase in pH and decrease in pCO_2 when compared to ambient levels, since full natural equilibration throughout the experiment
510
515 did not occur.

In this ~~particular~~ study, the focus was to ascertain whether the microbial community, inhabiting a neritic system, would respond in terms of production and respiration rates during ~~an almost three-month~~ 53-day exposure to the aforementioned conditions. Besides, differences in the response to the calcium and silicate inputs caused by the mineral addition simulations ~~mentioned above~~
520 were expected too. Especially in terms of community composition with calcium-based OAE treatments through the hydrated lime “addition” simulation (with compounds containing Ca^{2+} and OH^- separately), potentially increasing the abundance of pelagic calcifiers, and silicate-based OAE through the forsterite “addition” one (with compounds containing Mg^{2+} , SiO_3^{2-} , and OH^- independently), favoring diatom proliferation (Bach et al., 2019b). The latter community shifts
525 were predicted to yield distinct responses in terms of absolute community metabolic rates (gross

production, GP; net community production, NCP; community respiration, CR)s, and production efficiency via clear differences in assimilation numbers ($GP:Chla$) over time.

4.1 Response to the carbonate chemistry conditions: ~~Non-equilibrated TA gradient and to the mineral type~~

530 ~~Our results~~ results showed that OAE effects on microbial metabolic rates ~~was~~ may have been linked to nutrient availability. ~~The experiment was started commenced~~ Under the initial low inorganic nutrient concentrations (Figure 2), characteristic of post-bloom conditions (Figure 2). ~~Nutrient concentrations were low when the treatments were applied.~~ Thus, an initial response ~~in of~~ the microbial community production and respiration rates to the TA manipulation was likely

535 concealed by the nutrient limitation. ~~After~~ ~~Actually, after~~ ~~the~~ Following a simulated mixing event ~~a mixing event was simulated~~ on days 26 and 28, and the consequent nutrient enhancement, ~~however,~~ a response ~~could be discerned~~ discernible response pattern emerged. Blooms occurred in all ~~meseosmesmesocosms~~ despite the carbonate chemistry conditions. ~~s~~ Suggesting that the phytoplankton community were resilient to a TA manipulation of up to $600 \mu\text{mol L}^{-1}$.

540 ~~Nevertheless,~~ the most striking ~~noteworthy~~ result of our experiment is the inferred ~~The results from the current study though show a potential~~ delay in bloom formation with increasing TA, ~~when such manipulation is non-equilibrated.~~ ~~This delay is, although not significantly, longer in the calcium than in the silicate treatments.~~ ~~Meaning that the low-silicate treatments responded slightly earlier to the nutrient addition, than the low calcium ones.~~

545 In the past, ~~before ocean acidification emerged as a central focus of scientific research~~ ~~prior to the emergence of ocean acidification as a focal point in scientific inquiry~~, several culture experiments simulating high pH/low CO_2 conditions were carried out. For instance, Goldman (1999) ~~carried out~~ 12-day pH-drift, batch culture experiments, with three large diatom species (*Stephanopyxis palmeriana*, *Ditylum brightwelli* and *Cosinodiscus* sp.) and found that, when pH rose to above

550 8.5, growth rates started to decline. Similarly, Hansen (2002) performed 7-day experiments with three dinoflagellate species to evaluate their response in terms of growth rates and community succession. These were exposed to a pH range of 7.5 – 10, applied through the addition of NaOH , to simulate the conditions in the Mariager Fjord, Denmark. In these experiments, the three species' growth rates were the highest at pH 7.5, and a decrease to a 20% of the maximum growth rate

555 was observed at pH 8.3-8.5 for *Certaium lineatum*, and at 8.8–8.9 for *Heterocapsa triquetra* and *Prorocentrum minimum*. The latter also showed different tolerance limits, specifically 8.8, 9.5, and 9.6, respectively.

Additionally, despite the lack of data from experiments performed at constant pH at the time, Hansen (2002) compared his results with literature data on 35 species of marine phytoplankton

560 and concluded that there was high variability in their tolerance to high pH (8.4-10). Even within

the same family, species-specific tolerance limits could be observed. Most of these species would have been able to grow past the levels reached in the present study (half could grow above pH 9.2), but their growth rates would ~~possibly~~ decrease, at different species-specific levels, in relation to the increased pH (Chen & Durbin, 1994; Hansen, 2002). Therefore, offering the main explanation behind the qualitatively described delay in bloom formation ~~detected here~~. Although information on the species composition will be essential to fully evaluate the latter trend.

High extracellular pH can alter key membrane transport processes and metabolic functions involved in pH regulation (Smith and Raven, 1979). It can also induce changes in cellular amino acid relative composition and overall content (Søderberg and Hansen, 2007). But ~~an~~ key ~~associated~~ variable behind the response in terms of production observed in the ~~present-current~~ study is the inter-speciation of inorganic carbon ~~caused by~~ associated with the non-equilibrated nature of the TA manipulation. At pH 8, $\sim 1\%$ of the DIC in seawater is present as CO_2 , but at pH 9, this percentage is reduced 10 times over (Hansen, 2002). Additionally, 95% of the carbon fixation in the ocean is undertaken by the photosynthetic carbon-fixation reaction mediated by the RUBISCO (ribulose biphosphate carboxylase oxygenase) enzyme, which can only employ CO_2 (Raven, 2000). Thus, besides the pH levels reached here being around 8.7 in the highest treatments (calcium and silicate $\Delta 600 \mu\text{mol} \cdot \text{L}^{-1}$), which ~~we~~ are well above the maximum of 8.2 measured by Omar et al. (2019) in early spring (from 2005 to 2009) along the Norwegian west coast (~~particularly specifically in~~ Raunefjorden, our study site's location, as well as in Korsfjorden, Langenuen, and southern parts of the Hardangerfjorden), the associated low $p\text{CO}_2$ ~~$p\text{CO}_2$~~ attained was likely the detrimental treatment variable. Notably, the Chl a concentration, a proxy for phytoplankton biomass, was higher inside the mesocosms than in the fjord during phase II (Figure 3). This suggests that certain species may have thrived under the altered carbonate chemistry conditions present in the mesocosms. However, the microbial community in these mesocosms exhibited lower oxygen production per unit of Chl a , indicating that, despite an increase in phytoplankton biomass, the microbial community under high pH/low $p\text{CO}_2$ conditions may have been less efficient in terms of production than the one in the fjord (Figure 7).

Although CO_2 is the main substrate for photosynthesis ~~although~~, in its absence, many marine phytoplankton species adapt by using HCO_3^- through ~~carbon~~ Carbon ~~c~~ Concentrating ~~m~~ Mechanisms (CCMs; ~~(Giordano et al., 2005)~~). The latter are more energetically costly because they entail the concentration of HCO_3^- at the diffusion range of the plasma membrane, and the catalysis of ~~the~~ HCO_3^- to CO_2 for posterior CO_2 fixation. Thus, these pathways are less efficient, causing reduced ~~the mentioned~~ growth rates, and the subsequent delay in bloom formation with increasing TA without pre-equilibration (higher pH/lower CO_2 conditions) ~~observed~~. Although the response pattern found was described qualitatively due to the lack of statistical strength (small

sample size of the mineral treatments, n = 5, when considered separately) in the experimental design, it could be a relevant finding, granting further evaluation.

4.2 Response to the two simulated mineral additions: Calcium- vs silicate-based

600 The observed delay was, although not significantly, longer in the calcium than in the silicate treatments. Meaning that the low silicate treatments responded slightly earlier to the nutrient addition, than the low calcium ones. Besides the three-day lag noticed for the calcium treatments' response to the nutrient addition with respect to that of the silicate ones, and despite assimilation numbers showing no response to the TA gradient in either case, several differences between the two mineral treatments were noticed. Mildly higher production rates and Chl*a* concentrations
605 were observed in the silicate treatments when compared to the calcium ones. Both silicate and calcium treatment sets' microphytoplankton fractions included diatoms, in different proportions based on the mineral treatment, during the second phase were likely dominated by diatoms (Ferderer et al., 2023; Kittu et al., 2024, in prep).

Small diatoms are usually well adapted to post-bloom conditions due to their favorable surface to
610 volume ratio, an adaptation to low nutrient concentrations (Raven, 1986), and their well-developed CCMs (Chrachri et al., 2018). ~~Additionally, Daniels et al. (2015) studied the phytoplankton community structure dynamics during the early stages of the 2012 North Atlantic spring bloom. They noticed that, in the Norwegian Basin, the diatom community was dominated by nano-sized diatoms. If the same occurred in the present study~~ The acclimation to the carbonate chemistry conditions during phase I, coupled with exposure to high concentrations of silicate in the silicate treatments (positive slopes in daily linear models between Δ TA on GP:CR during phase I; Figure 6 A), would explain the faster response after the nutrient addition and the vast silicate uptake in the silicate treatments during phase II observed was of { Si:N ~10.7: 3.7 μ M, suggesting the community may have been diatom dominated), when compared to the calcium treatments. In the latter While in the calcium treatments, the community was silicate limited, in terms of nutrient uptake. ~~All the orthosilicate, as well as the to nitrate were, introduced to the system were~~ consumed in a ~1: 3.6 μ M Si:N-ratio. Diatoms have been observed to reduce their silicon requirements by exhibiting frustule thinning if exposed to silicate-limiting conditions to prioritize growth (McNair et al., 2018). In fact, Ferderer et al. (2023) found that diatoms in the
625 silicate treatments were more heavily silicified than in the calcium ones, generally independently of the TA level. Diatoms in these treatments may thus have been able to allocate more resources to growth and photosynthesis (Inomura et al., 2023). Therefore, the excess availability of silicate, coupled with acclimation to the carbonate chemistry during phase I, could have aided the faster response to the mixing event simulation, as well as contributed to the higher absolute GP and Chl*a* concentrations observed in the silicate treatments. ~~Which could potentially explain the~~

~~further delayed response to the mixing event simulation and the mildly lower absolute GP and Chla concentration observed in phase II when compared to the silicate treatments.~~

Further differences between mineral treatments could be inferred in the effect size of ΔTA on CR rates over time, which translated to differences in the effect of ΔTA on metabolic balance (GP:CR), in the second phase. A potential explanation for these results is likely in relation to differences in the phytoplankton community composition between the two sets of treatments. Notably, Ferderer et al. (2023) found that the effect of the mineral on silicification varied ~~between~~ among diatom genera in the same experiment. ~~However~~ Furthermore, even if the community ~~included was dominated by~~ diatoms, rapid diatom growth during a spring bloom does not necessarily suppress other non-diatom phytoplankton growth (Barber and Hiscock, 2006; Lochte et al., 1993). The latter may increase in absolute cell concentrations ~~and in terms of growth rates~~, but their absolute contribution to the total biomass when diatoms are abundantly present ~~is moderate could be modest~~ (Barber and Hiscock, 2006). This would therefore explain why, ~~when GP is normalized to Chla (assimilation numbers)~~, no differences between mineral treatments ~~and the response pattern observed in terms of GP and Chla, cannot can~~ be inferred, even if they occurred ~~in, in the absolute- assimilation number (GP:Chla) temporal development, nor in their~~ the aforementioned parameters' overtime response to the ΔTA gradient (Figure 7). It is though likely that the non-diatom phytoplankton community, both in terms of composition and contribution, differed between mineral treatments.

Lastly, the silicate control ~~behaved differently than did not behave as~~ expected. The increase in production and in Chla concentrations in the form of a large peak, as in all other treatments after ~~said the inorganic nutrient~~ addition, was not observed. Instead, both in terms of GP and Chla, two small peaks, a half in magnitude when compared to the calcium control, were noted. The observed discrepancy between the controls was unanticipated and may have resulted from a random response attributable to the mesocosm effect. Indeed, in this treatment, the absolute CR (Figure 5) and its contribution to GP right before the nutrient addition was the highest when compared to the rest. This difference between the controls was unexpected. This was probably a random response caused by the mesocosm effect. When communities are enclosed, even if initially they are very similar, they are not exactly the same and, over time, they may behave differently. The pre-addition phase allows for acclimation, but though it is held as short as possible ~~in order to~~ keep a similar community when the treatment is applied. However, it is still a bias to be taken into consideration.

4.3.2 Potential implications and future research

Given the novelty of this field and the findings from the current study, we outline ~~herein~~ some of the remaining unresolved research questions. Trophic decoupling between phytoplankton and

zooplankton has been observed in a large temperate lake where *Daphnia* resting eggs were unaffected by temperature increase while the phytoplankton spring bloom occurred earlier in the year (Winder and Schindler, 2004). This led to a long-term decline of *Daphnia*, the keystone ~~herbivore~~herbivorous zooplankton species, due to the increased mismatch with the spring bloom.

670 The opposite could be expected due to the observed delay in bloom development associated with the non-equilibrated OAE implementation. That is if micro- and mesozooplankton do not respond to the pH levels attained themselves, favoring trophic transfer. ~~In this experiment however, the zooplankton response was not observed due to the late formation of the bloom and the time scale of the experiment.~~ Considering that the transport of particulate organic matter to depth is regulated
675 by the coupling of primary and secondary producers (Wassmann, 1998), thus potentially affecting the OAE's CDR efficiency, this is a key implication that ~~requires~~may require further assessment.

Additionally, if the carbonate chemistry conditions were altered under pre-bloom or blooming conditions, the initial shock without prior acclimation may be stronger. It could potentially translate to longer delays in bloom development with increasing TA, and even changes in
680 community composition and overall production efficiency at certain alkalinity levels. Consequently, in turn possibly affecting trophic transfer and carbon export.

Finally, we hypothesize that the delayed response observed in relation to the TA manipulation would likely be amplified if higher non-equilibrated alkalinity additions were deployed. ~~Thus~~Although, in real-world applications, carbonate chemistry alterations may be transient and
685 less extreme, experiments that look into i) how and when absolute community metabolic rates respond to stronger higher TA levels~~OAE deployments~~, ii) where the threshold in the higher range of the gradient at which reduced GP:Chl*a* ratio~~community shift~~ could be induced is, but also iii) if a recovery could occur after a long-term exposure, or after dilution (short-term), are essential if safe deployment ~~safe~~ limits are to be identified.

690

5. CONCLUSIONS

This study presents the first experimental evaluation of the effects of a non-equilibrated, silicate vs calcium-~~based~~ OAE deployment under natural conditions, and at a mesocosm scale, on microbial metabolic rates. The total alkalinity (TA) manipulation (a silicate and a calcium based
695 five-step Δ TA gradients 0 – 600 $\mu\text{mol} \cdot \text{L}^{-1}$), without prior CO_2 sequestration, resulted in a stable increase in pH and a decrease in $p\text{CO}_2$. ~~that persisted~~persisting until the end of the experiment. Conducted in a neritic system under post-bloom conditions, ~~and~~ a mixing event was simulated roughly halfway through ~~it~~. Following the ~~addition of~~ inorganic nutrient addition, a mild delay in bloom formation, based on gross and net community production (GP and NCP) rates, and
700 chlorophyll *a* (Chl*a*) concentrations, in relation to the Δ TA gradient, was observed. Low TA

treatments responded slightly earlier than high TA ones, with the delay being longer for the calcium ~~treatment~~ compared to the silicate treatments ~~set~~. This delay is likely linked to the previously reported, species-specific negative relationship between high pH/low $p\text{CO}_2$ ~~pCO₂~~ conditions and phytoplankton growth rates. Although, overall, phytoplankton were resilient to the TA levels attained.

Seasonal differences in this pattern require further investigation, as nutrient limitation may ~~have concealed~~ have concealed a potentially more pronounced, short-term response to the TA addition. Given the qualitative nature of the observed described trend, additional experiments testing it further through, for instance, higher resolution gradients, are necessary. Further, while real-world OAE applications ~~of OAE~~ are expected to result in more transient and less extreme carbonate chemistry perturbations, a thorough assessment of TA limits is crucial. Particularly because ~~the~~ detected responses may become more pronounced at higher TA levels and vary depending on microbial species composition. Therefore, ~~are attained~~. Thus, ~~additional experiments studies under pre-blooming and blooming conditions to~~ evaluating recovery ~~to~~ from intense more intense carbonate chemistry ~~manipulations perturbations are~~ will be essential to establish safe TA addition limits for future OAE implementations.

Data availability

The dataset of the metabolic rates used in this study can be found in the online repository PANGAEA. Data can be accessed via the following link: <https://doi.org/10.1594/PANGAEA.972371> ~~The raw data~~ (Marín-Samper et al., 2024b). The chlorophyll *a*, carbonate chemistry and inorganic nutrient concentration data will be made available in the same repository. ~~supporting the conclusions of this article will be made available in a public data repository by the authors, without undo reservation.~~

Author contributions

Experimental concept and design: UR and JA. Direct participation in the experiment: LMS, JA and UR. Data analyses: LMS with input from NHH. Original draft preparation: LMS. Review and editing: All authors.

Financial support

This research has been supported by the Horizon 2020 Research and Innovation Programme project OceanNETs (“Ocean-based Negative Emissions Technologies – analysing the feasibility, risks and cobenefits of ocean-based negative emission technologies for stabilizing the climate”, grant no. 869357), and by the EU H2020-INFRAIA’s project AQUACOSM (“AQUACOSM: Network of Leading European AQUATic MesoCOSM Facilities Connecting Mountains to Oceans from the Arctic to the Mediterranean”, Project No.: 731065). Further, it was co-financed by the “Agencia Canaria de Investigación, Innovación y Sociedad de la Información” (ACIISI) of the “Consejería de Economía, Conocimiento y Empleo”, and by the “Fondo Social Europeo (FSE) Programa Operativo Integrado de Canarias 2014-2020, Eje 3 Tema Prioritario 74 (85%)”.

Competing interests

The authors declare that they have no conflict of interest.

Acknowledgements

The authors would like to express their most sincere gratitude to the entire KOSMOS team at GEOMAR for their invaluable support in managing logistics and, to the technical team for all the hard work building and maintaining the mesocosms during the campaign. Special appreciation is extended to ~~said team's~~their dedication in coordinating on-site research activities and fostering fair data management and exchange. A special thank you goes to Acorayda González from the biological oceanography group (GOB-ULPGC), for helping with the oxygen measurements. Also, we would like to ~~acknowledge~~commend Julieta Schneider (GEOMAR) and Kai Shulz (Southern Cross University) for the carbonate chemistry measurements, Juliane Tammen for the inorganic nutrient concentration data, and Leila Kittu (GEOMAR) Xiaoke Xin, Phillip Süßle, and Joaquin Ortiz for the interesting discussions on data interpretation. ~~Finally, we~~We also want to thank the University of Bergen for providing the Espeyrend Marine Research Field Station to conduct the experiment, and the station’s staff for all their assistance throughout. Lastly, we would like to acknowledge the three anonymous reviewers that contributed to improving this manuscript’s quality through their insightful feedback.

References

(IPCC), I. P. on C. C. (Ed.): Global Carbon and Other Biogeochemical Cycles and Feedbacks, in: Climate Change 2021 – The Physical Science Basis: Working Group I Contribution to the Sixth Assessment Report of the Intergovernmental Panel on Climate Change, Cambridge University Press, Cambridge, 673–816, <https://doi.org/DOI: 10.1017/9781009157896.007>, 2023.

- Albright, R., Caldeira, L., Hosfelt, J., Kwiatkowski, L., Maclaren, J. K., Mason, B. M., Nebuchina, Y., Ninokawa, A., Pongratz, J., Ricke, K. L., Rivlin, T., Schneider, K., Sesboüé, M., Shamberger, K., Silverman, J., Wolfe, K., Zhu, K., and Caldeira, K.: Reversal of ocean acidification enhances net coral reef calcification, *Nature*, 531, 362–365, <https://doi.org/10.1038/nature17155>, 2016.
- 770
- Bach, L. T., Gill, S. J., Rickaby, R. E. M., Gore, S., and Renforth, P.: CO₂ Removal With Enhanced Weathering and Ocean Alkalinity Enhancement: Potential Risks and Co-benefits for Marine Pelagic Ecosystems, *Front. Clim.*, 1, <https://doi.org/10.3389/fclim.2019.00007>, 2019a.
- 775
- Bach, L. T., Gill, S. J., Rickaby, R. E. M., Gore, S., and Renforth, P.: CO₂ Removal With Enhanced Weathering and Ocean Alkalinity Enhancement: Potential Risks and Co-benefits for Marine Pelagic Ecosystems, *Front. Clim.*, 1, 7, <https://doi.org/10.3389/fclim.2019.00007>, 2019b.
- Barber, R. T. and Hiscock, M. R.: A rising tide lifts all phytoplankton: Growth response of other phytoplankton taxa in diatom-dominated blooms, *Global Biogeochem. Cycles*, 20, 1–12, <https://doi.org/10.1029/2006GB002726>, 2006.
- 780
- Carpenter, C. and: Modifications Employed of the Winkler Method for Determining Dissolved Oxygen in Seawater ; A NASCO Report ', 1966.
- Chen, C. Y. and Durbin, E. G.: Effects of pH on the growth and carbon uptake of marine phytoplankton, *Mar. Ecol. Prog. Ser.*, 109, 83–94, <https://doi.org/10.3354/meps109083>, 1994.
- 785
- Chen, S. M., Riebesell, U., Schulz, K. G., Von Der Esch, E., Achterberg, E. P., and Bach, L. T.: Temporal dynamics of surface ocean carbonate chemistry in response to natural and simulated upwelling events during the 2017 coastal El Niño near Callao, Peru, *Biogeosciences*, 19, 295–312, <https://doi.org/10.5194/bg-19-295-2022>, 2022.
- Chrachri, A., Hopkinson, B. M., Flynn, K., Brownlee, C., and Wheeler, G. L.: Dynamic changes in carbonate chemistry in the microenvironment around single marine phytoplankton cells, *Nat. Commun.*, 9, 1–12, <https://doi.org/10.1038/s41467-017-02426-y>, 2018.
- 790
- Czerny, J., Schulz, K. G., Krug, S. A., Ludwig, A., and Riebesell, U.: Technical note: The determination of enclosed water volume in large flexible-wall mesocosms KOSMOS, *Biogeosciences*, 10, 1937–1941, <https://doi.org/10.5194/bg-10-1937-2013>, 2013.
- 795
- Dickson, A., Sabine, C., and Christian, J.: Guide to Best Practices for Ocean CO₂ Measurements, PICES Special Publication 3, 191 pp., 2007.
- Feng, E. Y., Koeve, W., Keller, D. P., and Oschlies, A.: Model-Based Assessment of the CO₂ Sequestration Potential of Coastal Ocean Alkalinization, *Earth's Futur.*, 5, 1252–1266, <https://doi.org/10.1002/2017EF000659>, 2017.

800 Ferderer, A., Schulz, K. G., Riebesell, U., Baker, K. G., Chase, Z., and Bach, L. T.: Investigating the effect of silicate and calcium based ocean alkalinity enhancement on diatom silicification, *Biogeosciences Discuss.*, 1–28, 2023.

Friedlingstein, P., Jones, M. W., O’Sullivan, M., Andrew, R. M., Hauck, J., Peters, G. P., Peters, W., Pongratz, J., Sitch, S., Le Quéré, C., Bakker, D. C. E., Canadell, J. G., Ciais, P., Jackson, R. B., Anthoni, P., Barbero, L., Bastos, A., Bastrikov, V., Becker, M., Bopp, L., Buitenhuis, E., Chandra, N., Chevallier, F., Chini, L. P., Currie, K. I., Feely, R. A., Gehlen, M., Gilfillan, D., Gkritzalis, T., Goll, D. S., Gruber, N., Gutekunst, S., Harris, I., Haverd, V., Houghton, R. A., Hurtt, G., Ilyina, T., Jain, A. K., Joetzjer, E., Kaplan, J. O., Kato, E., Klein Goldewijk, K., Korsbakken, J. I., Landschützer, P., Lauvset, S. K., Lefèvre, N., Lenton, A., Lienert, S., Lombardozzi, D., Marland, G., McGuire, P. C., Melton, J. R., Metzl, N., Munro, D. R., Nabel, J. E. M. S., Nakaoka, S.-I., Neill, C., Omar, A. M., Ono, T., Peregón, A., Pierrot, D., Poulter, B., Rehder, G., Resplandy, L., Robertson, E., Rödenbeck, C., Séférian, R., Schwinger, J., Smith, N., Tans, P. P., Tian, H., Tilbrook, B., Tubiello, F. N., van der Werf, G. R., Wiltshire, A. J., and Zaehle, S.: Global Carbon Budget 2019, *Earth Syst. Sci. Data*, 11, 1783–1838, <https://doi.org/10.5194/essd-11-1783-2019>, 2019.

Friedlingstein, P., Jones, M. W., O’Sullivan, M., Andrew, R. M., Bakker, D. C. E., Hauck, J., Le Quéré, C., Peters, G. P., Peters, W., Pongratz, J., Sitch, S., Canadell, J. G., Ciais, P., Jackson, R. B., Alin, S. R., Anthoni, P., Bates, N. R., Becker, M., Bellouin, N., Bopp, L., Chau, T. T. T., Chevallier, F., Chini, L. P., Cronin, M., Currie, K. I., Decharme, B., Djeutchouang, L. M., Dou, X., Evans, W., Feely, R. A., Feng, L., Gasser, T., Gilfillan, D., Gkritzalis, T., Grassi, G., Gregor, L., Gruber, N., Gürses, Ö., Harris, I., Houghton, R. A., Hurtt, G. C., Iida, Y., Ilyina, T., Luijkx, I. T., Jain, A., Jones, S. D., Kato, E., Kennedy, D., Goldewijk, K. K., Knauer, J., Korsbakken, J. I., Körtzinger, A., Landschützer, P., Lauvset, S. K., Lefèvre, N., Lienert, S., Liu, J., Marland, G., McGuire, P. C., Melton, J. R., Munro, D. R., Nabel, J. E. M. S., Nakaoka, S. I., Niwa, Y., Ono, T., Pierrot, D., Poulter, B., Rehder, G., Resplandy, L., Robertson, E., Rödenbeck, C., Rosan, T. M., Schwinger, J., Schwingshackl, C., Séférian, R., Sutton, A. J., Sweeney, C., Tanhua, T., Tans, P. P., Tian, H., Tilbrook, B., Tubiello, F., Van Der Werf, G. R., Vuichard, N., Wada, C., Wanninkhof, R., Watson, A. J., Willis, D., Wiltshire, A. J., Yuan, W., Yue, C., Yue, X., Zaehle, S., and Zeng, J.: Global Carbon Budget 2021, *Earth Syst. Sci. Data*, 14, 1917–2005, <https://doi.org/10.5194/essd-14-1917-2022>, 2022.

Fuss, S., Canadell, J. G., Ciais, P., Jackson, R. B., Jones, C. D., Lyngfelt, A., Peters, G. P., and Van Vuuren, D. P.: Moving toward Net-Zero Emissions Requires New Alliances for Carbon Dioxide Removal, *One Earth*, 3, 145–149, <https://doi.org/10.1016/j.oneear.2020.08.002>, 2020.

Gafar, N. A. and Schulz, K. G.: A three-dimensional niche comparison of *Emiliania huxleyi* and

- 835 *Gephyrocapsa oceanica*: Reconciling observations with projections, *Biogeosciences*, 15, 3541–3560, <https://doi.org/10.5194/bg-15-3541-2018>, 2018.
- Gattuso, J. P., Magnan, A. K., Bopp, L., Cheung, W. W. L., Duarte, C. M., Hinkel, J., Mcleod, E., Micheli, F., Oschlies, A., Williamson, P., Billé, R., Chalastani, V. I., Gates, R. D., Irisson, J. O., Middelburg, J. J., Pörtner, H. O., and Rau, G. H.: Ocean solutions to address climate change and its effects on marine ecosystems, *Front. Mar. Sci.*, 5, <https://doi.org/10.3389/fmars.2018.00337>, 2018.
- Gilpin, L. C., Davidson, K., and Roberts, E.: The influence of changes in nitrogen: silicon ratios on diatom growth dynamics, *J. Sea Res.*, 51, 21–35, <https://doi.org/https://doi.org/10.1016/j.seares.2003.05.005>, 2004.
- 845 Giordano, M., Beardall, J., and Raven, J. A.: CO₂ concentrating mechanisms in algae: Mechanisms, environmental modulation, and evolution, *Annu. Rev. Plant Biol.*, 56, 99–131, <https://doi.org/10.1146/annurev.arplant.56.032604.144052>, 2005.
- Goldman, J. C.: Inorganic carbon availability and the growth of large marine diatoms, *Mar. Ecol. Prog. Ser.*, 180, 81–91, <https://doi.org/10.3354/meps180081>, 1999.
- 850 Grasshof, K., Kremling, K., and Ehrhard, M.: Arsenic , antimony , and germanium , in *Methods of Seawater Analysis* edited, Wiley-VCH, Weinheim, 274–294, 1999.
- Hansen, H. P. and Koroleff, F.: Determination of nutrients, *Methods seawater Anal.*, 159–228, 1999.
- Hansen, P. J.: Effect of high pH on the growth and survival of marine phytoplankton: implications for species succession, 28, 279–288, 2002.
- 855 Hartmann, J., Suitner, N., Lim, C., Schneider, J., Marín-Samper, L., Arístegui, J., Renforth, P., Taucher, J., and Riebesell, U.: Stability of alkalinity in ocean alkalinity enhancement (OAE) approaches - consequences for durability of CO₂ storage, *Biogeosciences*, 20, 781–802, <https://doi.org/10.5194/bg-20-781-2023>, 2023.
- 860 Harvey, L. D. D.: Mitigating the atmospheric CO₂ increase and ocean acidification by adding limestone powder to upwelling regions, *J. Geophys. Res. Ocean.*, 113, 1–21, <https://doi.org/10.1029/2007JC004373>, 2008.
- Hauck, J., Köhler, P., Wolf-Gladrow, D., and Völker, C.: Iron fertilisation and century-scale effects of open ocean dissolution of olivine in a simulated CO₂ removal experiment, *Environ. Res. Lett.*, 11, <https://doi.org/10.1088/1748-9326/11/2/024007>, 2016.
- 865 Holmes, R. M., Aminot, A., Kérouel, R., Hooker, B. A., and Peterson, B. J.: A simple and precise method for measuring ammonium in marine and freshwater ecosystems, *Can. J. Fish. Aquat. Sci.*,

- 56, 1801–1808, <https://doi.org/10.1139/f99-128>, 1999.
- Inomura, K., Pierella Karlusich, J. J., Dutkiewicz, S., Deutsch, C., Harrison, P. J., and Bowler,
870 C.: High Growth Rate of Diatoms Explained by Reduced Carbon Requirement and Low Energy
Cost of Silica Deposition, *Microbiol. Spectr.*, 11, <https://doi.org/10.1128/spectrum.03311-22>,
2023.
- IPCC: Global warming of 1.5°C, 228–231 pp., 2018.
- IPCC: Climate Change 2022: Mitigation of Climate Change. Contribution of Working Group III
875 to the Sixth Assessment Report of the Intergovernmental Panel on Climate Change, 1–30 pp.,
2022.
- Jones, D. C., Ito, T., Takano, Y., and Hsu, W. C.: Spatial and seasonal variability of the air-sea
equilibration timescale of carbon dioxide, *Global Biogeochem. Cycles*, 28, 1163–1178,
<https://doi.org/10.1002/2014GB004813>, 2014.
- 880 Kheshgi, H. S.: Sequestering atmospheric carbon dioxide by increasing ocean alkalinity, *Energy*,
20, 915–922, [https://doi.org/10.1016/0360-5442\(95\)00035-F](https://doi.org/10.1016/0360-5442(95)00035-F), 1995.
- Köhler, P., Abrams, J. F., Völker, C., Hauck, J., and Wolf-Gladrow, D. A.: Geoengineering
impact of open ocean dissolution of olivine on atmospheric CO₂, surface ocean pH and marine
biology, *Environ. Res. Lett.*, 8, <https://doi.org/10.1088/1748-9326/8/1/014009>, 2013.
- 885 Lee, J.-Y., J. Marotzke, G. Bala, L. Cao, S. Corti, J.P. Dunne, F. Engelbrecht, E. Fischer, J.C.
Fyfe, C. Jones, A. Maycock, J. Mutemi, O. Ndiaye, S. Panickal, and T. Zhou: Future Global
Climate: Scenario-Based Projections and Near-Term Information, 553–672 pp.,
<https://doi.org/10.1017/9781009157896.006.553>, 2021.
- Lewis, E. and Wallace, D.: Program Developed for CO₂ System Calculations ORNL/CDIAC-
890 105, Carbon Dioxide Information Analysis Centre, 1998.
- Lochte, K., Ducklow, H. W., Fasham, M. J. R., and Stienen, C.: Plankton succession and carbon
cycling at 47°N 20°W during the JGOFS North Atlantic Bloom Experiment, *Deep Sea Res. Part
II Top. Stud. Oceanogr.*, 40, 91–114, [https://doi.org/10.1016/0967-
0645\(93\)90008-B](https://doi.org/10.1016/0967-0645(93)90008-B), 1993.
- 895 Marín-Samper, L., Arístegui, J., Hernández-Hernández, N., Ortiz, J., Archer, S. D., Ludwig, A.,
and Riebesell, U.: Assessing the impact of CO₂ equilibrated ocean alkalinity enhancement on
microbial metabolic rates in an oligotrophic system, *EGUsphere*, 2024, 1–29, 2024a.
- Marín-Samper, L., Arístegui, J., Hernández-Hernández, N., and Riebesell, U.: KOSMOS 2022
Bergen mesocosm study on ocean alkalinity enhancement: phytoplankton metabolic rates,
900 <https://doi.pangaea.de/10.1594/PANGAEA.972371>, 2024b.

- McNair, H. M., Brzezinski, M. A., and Krause, J. W.: Diatom populations in an upwelling environment decrease silica content to avoid growth limitation, *Environ. Microbiol.*, 20, 4184–4193, <https://doi.org/10.1111/1462-2920.14431>, 2018.
- 905 Montserrat, F., Renforth, P., Hartmann, J., Leermakers, M., Knops, P., and Meysman, F. J. R.: Olivine Dissolution in Seawater: Implications for CO₂ Sequestration through Enhanced Weathering in Coastal Environments, *Environ. Sci. Technol.*, 51, 3960–3972, <https://doi.org/10.1021/acs.est.6b05942>, 2017.
- 910 O'Neill, B. C., Tebaldi, C., Van Vuuren, D. P., Eyring, V., Friedlingstein, P., Hurtt, G., Knutti, R., Kriegler, E., Lamarque, J.-F., and Lowe, J.: The scenario model intercomparison project (ScenarioMIP) for CMIP6, *Geosci. Model Dev.*, 9, 3461–3482, 2016.
- Omar, A. M., Skjelvan, I., Erga, S. R., and Olsen, A.: Aragonite saturation states and pH in western Norwegian fjords: Seasonal cycles and controlling factors, 2005-2009, *Ocean Sci.*, 12, 937–951, <https://doi.org/10.5194/os-12-937-2016>, 2019.
- 915 Paul, A. J. and Bach, L. T.: Universal response pattern of phytoplankton growth rates to increasing CO₂, *New Phytol.*, 228, 1710–1716, <https://doi.org/10.1111/nph.16806>, 2020.
- Raven, J. A.: Physiological consequences of extremely small size for autotrophic organisms in the sea, *Canadian Bull. Fish. Aquat. Sci.*, 214, 1–70, 1986.
- Raven, J. A.: Limits on growth rates, *Nature*, 11, 438–443, 2000.
- 920 Raven, J. A. and Johnston, A.: Mechanisms of inorganic-carbon acquisition in marine phytoplankton and their implications for the use of other resources concentration on growth and photosynthesis by marine phytoplankton organisms has been little investigated relative to the effects me, 36, 1991.
- Renforth, P. and Henderson, G.: Assessing ocean alkalinity for carbon sequestration, *Rev. Geophys.*, 55, 636–674, <https://doi.org/10.1002/2016RG000533>, 2017.
- 925 Riebesell, U., Wolf-Gladrow, D. A., and Smetacek, V.: Carbon dioxide limitation of marine phytoplankton growth rates, *Nature*, 361, 249–251, <https://doi.org/10.1038/361249a0>, 1993.
- Riebesell, U., Czerny, J., Von Bröckel, K., Boxhammer, T., Büdenbender, J., Deckelnick, M., Fischer, M., Hoffmann, D., Krug, S. A., Lentz, U., Ludwig, A., Mucche, R., and Schulz, K. G.: Technical Note: A mobile sea-going mesocosm system - New opportunities for ocean change research, *Biogeosciences*, 10, 1835–1847, <https://doi.org/10.5194/bg-10-1835-2013>, 2013.
- 930 Rogelj, J., Popp, A., Calvin, K. V., Luderer, G., Emmerling, J., Gernaat, D., Fujimori, S., Strefler, J., Hasegawa, T., Marangoni, G., Krey, V., Kriegler, E., Riahi, K., van Vuuren, D. P., Doelman, J., Drouet, L., Edmonds, J., Fricko, O., Harmsen, M., Havlík, P., Humpenöder, F., Stehfest, E.,

- and Tavoni, M.: Scenarios towards limiting global mean temperature increase below 1.5 °C, *Nat. Clim. Chang.*, 8, 325–332, <https://doi.org/10.1038/s41558-018-0091-3>, 2018.
- Schuiling, R. D. and Krijgsman, P.: Enhanced weathering: An effective and cheap tool to sequester CO₂, *Clim. Change*, 74, 349–354, <https://doi.org/10.1007/s10584-005-3485-y>, 2006.
- Schulz, K. G., Bach, L. T., Bellerby, R. G. J., Bermúdez, R., Büdenbender, J., Boxhammer, T., Czerny, J., Engel, A., Ludwig, A., Meyerhöfer, M., Larsen, A., Paul, A. J., Sswat, M., and Riebesell, U.: Phytoplankton blooms at increasing levels of atmospheric carbon dioxide: Experimental evidence for negative effects on prymnesiophytes and positive on small picoeukaryotes, *Front. Mar. Sci.*, 4, <https://doi.org/10.3389/fmars.2017.00064>, 2017.
- Schulz, K. G., Bach, L. T., and Dickson, A. G.: Seawater carbonate system considerations for ocean alkalinity enhancement research, *State Planet Discuss.*, 1–24, <https://doi.org/10.5194/sp-2023-12>, 2023.
- Smith, F. A. and Raven, J. A.: AND ITS REGULATION, 1979.
- Søderberg, L. M. and Hansen, P. J.: Growth limitation due to high pH and low inorganic carbon concentrations in temperate species of the dinoflagellate genus *Ceratium*, 351, 103–112, <https://doi.org/10.3354/meps07146>, 2007.
- Taucher, J., Bach, L. T., Boxhammer, T., Nauendorf, A., Achterberg, E. P., Algueró-Muñiz, M., Arístegui, J., Czerny, J., Esposito, M., Guan, W., Haunost, M., Horn, H. G., Ludwig, A., Meyer, J., Spisla, C., Sswat, M., Stange, P., Riebesell, U., Aberle-Malzahn, N., Archer, S., Boersma, M., Broda, N., Büdenbender, J., Clemmesen, C., Deckelnick, M., Dittmar, T., Dolores-Gelado, M., Dörner, I., Fernández-Urruzola, I., Fiedler, M., Fischer, M., Fritsche, P., Gomez, M., Grossart, H. P., Hattich, G., Hernández-Brito, J., Hernández-Hernández, N., Hernández-León, S., Hornick, T., Kolzenburg, R., Krebs, L., Kreuzburg, M., Lange, J. A. F., Lischka, S., Linsenbarth, S., Löscher, C., Martínez, I., Montoto, T., Nachtigall, K., Osmá-Prado, N., Packard, T., Pansch, C., Posman, K., Ramírez-Bordón, B., Romero-Kutzner, V., Rummel, C., Salta, M., Martínez-Sánchez, I., Schröder, H., Sett, S., Singh, A., Suffrian, K., Tames-Espinosa, M., Voss, M., Walter, E., Wannicke, N., Xu, J., and Zark, M.: Influence of ocean acidification and deep water upwelling on oligotrophic plankton communities in the subtropical North Atlantic: Insights from an in situ mesocosm study, *Front. Mar. Sci.*, 4, <https://doi.org/10.3389/fmars.2017.00085>, 2017.
- Wassmann, P.: Retention versus export food chains: processes controlling sinking loss from marine pelagic systems, in: *Eutrophication in Planktonic Ecosystems: Food Web Dynamics and Elemental Cycling: Proceedings of the Fourth International PELAG Symposium, held in Helsinki, Finland, 26--30 August 1996*, edited by: Tamminen, T. and Kuosa, H., Springer Netherlands, Dordrecht, 29–57, https://doi.org/10.1007/978-94-017-1493-8_3, 1998.

- Welschmeyer, N. A.: Fluorometric analysis of chlorophyll a in the presence of chlorophyll b and pheopigments, *Limnol. Oceanogr.*, 39, 1985–1992, <https://doi.org/10.4319/lo.1994.39.8.1985>,
970 1994.
- Winder, M. and Schindler, D. E.: Climate change uncouples trophic interactions in an aquatic ecosystem, *Ecology*, 85, 2100–2106, <https://doi.org/10.1890/04-0151>, 2004.
- Xin, X., Faucher, G., and Riebesell, U.: Phytoplankton Response to Increased Nickel in the Context of Ocean Alkalinity Enhancement, *Biogeosciences Discuss.*, 2023, 1–15, 2023.
- 975 Zeebe, R. E. and Wolf-Gladrow, D.: CO₂ in seawater: equilibrium, kinetics, *Isot. Elsevier Sci. BV*, Amsterdam, Netherlands, 2001.

-